Pro gradu -tutkielma
Teoreettinen Fysiikka

Discrete Dipole Approximation for Thermal Radiation in Porous Media

Olli Vartia
2013

Ohjaaja:	Ari Seppälä
Tarkastajat:	Kari Rummukainen
	Ari Seppälä

HELSINGIN YLIOPISTO
FYSIIKAN LAITOS

PL 64 (Gustaf Hällströmin katu 2)
00014 Helsingin yliopisto

HELSINGIN YLIOPISTO – HELSINGFORS UNIVERSITET – UNIVERSITY OF HELSINKI

Tiedekunta/Osasto – Fakultet/Sektion – Faculty/Section	Laitos – Institution – Department	
Faculty of Science	Department of Physics	
Tekijä – Författare – Author		
Olli Santeri Vartia		
Työn nimi – Arbetets titel – Title		
Discrete Dipole Approximation for Thermal Radiation in Porous Media		
Oppiaine – Läroämne – Subject		
Theoretic Physics		
Työn laji – Arbetets art – Level	Aika – Datum – Month and year	Sivumäärä – Sidoantal – Number of pages
Pro Gradu	May 2013	45

Tiivistelmä – Referat – Abstract

Porous structures, such as foams make excellent thermal insulators. This happens because thermal transfer by conduction is hindered by the voids in the material. However, heat can still radiate through the material or just past the voids. Due to Stefan-Boltzmann law, heat transfer by radiation can be especially significant for large temperatures, and it follows that thermal transfer models that account for radiation may be necessary in some cases.

Several existing models for radiative thermal transfer in porous materials, such as continuum models and Monte Carlo, have been used in the past. What many of these models tend to have in common, is that they are highly specific to the systems they were originally made for and require some rather limiting approximations. A more general method which would only require knowing the material and the geometry of the system would be useful.

One candidate for such a method, discrete dipole approximation for periodic structures, was tested. In the discrete dipole approximation a structure is discretized into a collection of polarizable points, or dipoles and an incoming electromagnetic planewave is set to polarize it. This has the benefits that it accurately takes into account the target geometry and possible near field effects.

It was found that this method is limited for high wavelength, by computation time and for small wavelengths by errors. The cause of the errors for small wavelengths was not entirely caused by the discretization and remains not fully understood.

Avainsanat – Nyckelord – Keywords

discrete dipole approximation, thermal radiation, porous medium

Säilytyspaikka – Förvaringställe – Where deposited

Muita tietoja – Övriga uppgifter – Additional information

Contents

Chapter 1

Introduction

There are many reasons why being able to control thermal transfer is desirable. Buildings benefit from proper thermal insulation in form of reduced heating costs, refrigeration is more efficient with better insulation and many processes and machines produce heat, which can be a problem when they heat up things around them.

Porous structures, such as foams, are efficient thermal insulators, because the voids in the structure hinder thermal transfer by conduction. In the case of closed foams, heat transfer by convection is also reduced. Depending on the system, heat transfer by radiation can still be quite significant, especially for higher temperatures, and a model that accounts for it may be needed.

As will be discussed later in this thesis, many existing models for radiation in porous media simply treat the structure as if it were a semitransparent continuum, but these models require a number of approximations, which may not always be applicable. Models that attempt to take the structure into account do exist, but they tend to be very specific and some of them do not take into account effects caused by very small characteristic structure size.

The aim of this thesis is to first take a look at different methods of modeling thermal radiation in porous structures and then, more specifically explore the applicability of discrete dipole approximation in simulating scattering and absorption in porous structures. Using a method like this would have the advantage of potentially being able to model a system based on its structure and its materials' complex refractive index, while being able to account for effects caused by the structure being smaller or in same length scale as the wavelengths of the radiation.

Chapter 2

Theory

2.1 Background

The structure or especially the sub-wavelength structure of a block or a layer of material can have a significant effect on how radiation is transmitted through it. As an extreme example, sub-wavelength holes have been found, by Ebbesen et al., to increase transmission dramatically in a metallic film [14], but surprisingly also the complete opposite has been observed by Braun et al. [15] who found that an otherwise semitransparent metal film could be made to transmit less light with the addition of a square array of sub-wavelength holes. Nothing this extreme is expected here, but it is important to note that sub-wavelength structures can have an effect in how light is transmitted in a medium.

A number of existing models for thermal transfer by radiation in porous materials will be discussed in the following subsections. The first one discussed will be the Rosseland approximation, which is one of the existing continuum approximations that are sometimes used. This will be followed by the Monte-Carlo methods and finally methods which attempt to directly simulate the scattering and absorption of electromagnetic waves. Each of these methods have their own strengths and weaknesses and these subsections will help understand why the discrete dipole approximation was chosen to be used later on in this thesis.

2.1.1 Continuum treatments

This subsection will briefly discuss the heat transfer models, which approximate the structure of the system to be continuous, and the theory behind them. Especially the often used Rosseland diffusion equation is looked at.

According to Siegel and Howell [1], the change in spectral radiation intensity i'_λ with

respect to the solid angle $\mathrm{d}\omega$ about the direction S is

$$\begin{aligned}\frac{\mathrm{d}i'_\lambda}{\mathrm{d}S} =& -a_\lambda i'_\lambda(S) + a_\lambda i'_{\lambda b}(S) - \sigma_{s\lambda} i'_\lambda(S) \\ &+ \frac{\sigma_{s\lambda}}{4\pi}\int_{\omega_i=4\pi} i'_\lambda(S,\omega_i)\Phi(\lambda,\omega,\omega_i)\mathrm{d}\omega_i. \end{aligned} \tag{2.1}$$

The meanings of the terms on Eq. (2.1) are the following. The first term on the right, $a_\lambda i'_\lambda(S)$ accounts for the loss of intensity caused by absorption a_λ, which in this case also includes the effect of induced emission. The next similar looking term $a_\lambda i'_{\lambda b}(S)$ is the intensity gained through emission within $\mathrm{d}\omega$. However, it is important to note that the subscript b in $i'_{\lambda b}(S)$ signifies that this is spectral intensity due to blackbody radiation and is not to be mixed with i'_λ. The effect of induced emission is not included. Term $\sigma_{s\lambda} i'_\lambda(S)$, where $\sigma_{s\lambda}$ is the scattering coefficient, gives the intensity loss due to scattering. Finally the integral term $\frac{\sigma_{s\lambda}}{4\pi}\int_{\omega_i=4\pi} i'_\lambda(S,\omega_i)\Phi(\lambda,\omega,\omega_i)\mathrm{d}\omega_i$ gives the intensity gained by scattering. In this, ω_i is the solid angle of incoming radiation and $\Phi(\lambda,\omega,\omega_i)$ is the phase function which gives the portion of radiation of wavelength λ that is scattered from angle ω_i to angle ω.

The absorption and scattering coefficients in Eq. (2.1) may be combined to $K_\lambda = a_\lambda + \sigma_\lambda$, which is known as the extinction coefficient. Now if S is replaced with the optical thickness κ_λ using the relation

$$\mathrm{d}\kappa_\lambda = K_\lambda(S)\mathrm{d}S, \tag{2.2}$$

Eq. (2.1) may be written in a shorter form known as the *the radiative transfer equation*, or RTE:

$$\frac{\mathrm{d}i'_\lambda}{\mathrm{d}\kappa_\lambda} + i'_\lambda(\kappa_\lambda) = I'_\lambda(\kappa_\lambda,\omega) \tag{2.3}$$

In this new form $I'_\lambda(\kappa_\lambda,\omega)$ is the source function

$$I'_\lambda(\kappa_\lambda,\omega) = \frac{a_\lambda}{K_\lambda} i'_{\lambda b}(\kappa_\lambda) + \frac{\sigma_{s\lambda}}{4\pi K_\lambda}\int_{\omega_i=4\pi} i'_\lambda(\kappa_\lambda,\omega_i)\Phi(\lambda,\omega,\omega_i)\mathrm{d}\omega_i, \tag{2.4}$$

which contains both of the intensity gain terms of Eq. (2.1).

The radiative transfer equation (2.3) is an integro-differential equation and cannot in general be solved analytically. One approximative way to get around this is the *Rosseland diffusion equation* [1].

$$\frac{\mathrm{d}q_\lambda(x)}{\mathrm{d}\lambda} = -\frac{4\pi}{3K_\lambda(x)}\frac{\mathrm{d}i'_{\lambda b}}{\mathrm{d}x} = -\frac{4}{3K_\lambda(x)}\frac{\mathrm{d}e_{\lambda b}}{\mathrm{d}x} \tag{2.5}$$

Here $q_\lambda(x)$ is the energy flux generated by photons of wavelength λ at depth x in a slab of the medium. $e_{\lambda b}$ is Planck's distribution

$$e_{\lambda b}(\lambda) = \pi i'_{\lambda b}(\lambda) = \frac{2hc^2}{\lambda^5}\frac{1}{e^{\frac{hc}{\lambda kT}} - 1}. \tag{2.6}$$

The diffusion approximation only works if the medium is assumed to be optically thick, meaning that a photon may travel only for a short distance, compared to the size of the system, without being absorbed. Scattering is also assumed to be isotropic. If the medium can be thought to be gray, Eq. (2.5) may be further simplified following Siegel and Howell [1] and using the Stefan-Boltzmann law $\int \pi i'_{\lambda b} \mathrm{d}\lambda = e_b = \sigma T^4$ and integrating with respect to wavelength

$$\begin{aligned} q(x) &= -\frac{4\sigma}{3}\int \frac{1}{K_\lambda}\frac{\mathrm{d}e_{\lambda b}}{\mathrm{d}x}\mathrm{d}\lambda \\ &= -\frac{4\sigma}{3}\frac{\int (1/K_\lambda)(\mathrm{d}e_{\lambda b}/\mathrm{d}x)\mathrm{d}\lambda}{\int (\mathrm{d}e_{\lambda b}/\mathrm{d}x)\mathrm{d}\lambda}\int \frac{\mathrm{d}e_{\lambda b}}{\mathrm{d}x}\mathrm{d}\lambda \\ &= -\frac{4\sigma}{3}\frac{1}{K}\frac{\mathrm{d}e_b}{\mathrm{d}x} \\ &= -\frac{4\sigma}{3K}\frac{\mathrm{d}(T^4)}{\mathrm{d}x} \\ &= -\frac{16\sigma}{3K}T^3\frac{\mathrm{d}T}{\mathrm{d}x}. \end{aligned} \tag{2.7}$$

T is the temperature and σ is the Stefan-Boltzmann constant. *The Rosseland mean extinction coefficient* K_R as defined by Siegel and Howell [1]

$$\begin{aligned} \frac{1}{K_R} &= \frac{\int (1/K_\lambda)(\partial e_{\lambda b}/\partial x)\mathrm{d}\lambda}{\int (\partial e_{\lambda b}/\partial x)\mathrm{d}\lambda} \\ &= \frac{\int (1/K_\lambda)(\partial e_{\lambda b}/\partial x)(\partial x/\partial e_b)\mathrm{d}\lambda}{\int (\partial e_{\lambda b}/\partial x)(\partial x/\partial e_b)\mathrm{d}\lambda} \\ &= \frac{\int (1/K_\lambda)(\partial e_{\lambda b}/\partial e_b)\mathrm{d}\lambda}{\int (\partial e_{\lambda b}/\partial e_b)\mathrm{d}\lambda}, \end{aligned} \tag{2.8}$$

is the extinction coefficient that is usually used in Eq. (2.7) in place of K. K_R is essentially the average of the medium's extinction coefficient weighted by Planck's distribution (2.6) with respect to total emissive power over the spectrum $\int_{\Delta\lambda} \epsilon \mathrm{d}\lambda = \int_{\Delta\lambda} \partial e_{\lambda b}/\partial e_\lambda \mathrm{d}\lambda$.

Eq. (2.7) has the same form as Fourier's law for heat flux [1]

$$q = -k_{eff}\frac{\mathrm{d}T}{\mathrm{d}x} \tag{2.9}$$

and so $\frac{16\sigma}{3K}T^3 = k_r$ may be handily used as a component for the effective heat conductivity k_{eff} of the medium.

The usefulness of the Rosseland mean approach is naturally limited by the approximations that have to be made in order to use it. Since it is a continuum model it is only applicable to optically thick systems. Especially since Eq. (2.5) is one of the so called diffusion solutions to RTE, it as such ignores the effects of possible anisotropic scattering. This has been addressed for example by Doermann and Sacadura [3], Placido et al. [4] and Coquard et al. [5] who used a weighted extinction coefficients K_R^* instead of Eq. (2.8) to account for possible anisotropic effects. The weighted extinction coefficients were calculated assuming that the foam in question consists of differently shaped randomly oriented particles, such as cell walls and struts.

In Doermann's and Sacadura's paper [3] the particles are large compared to the wavelength of the radiation. Also the shapes of the particles only come in to play when determining the effect of diffraction on the phase function, for the effect of reflections the particle's are assumed to be spherical because of their random orientation. For multiple scattering the effect of diffraction is ignored, which means that the particle shapes are important only in the case of single scattering. On the other hand Placido et al. [4] do not differentiate diffraction from reflection, because they use Mie theory to calculate the extinction coefficients for the different particles used in their paper. Coquard et al. [5] used geometric optics, however their model also took into account the structure of their specific foam on a macroscopic level. None of the models above account for dependent scattering, which means that close by particles must not affect each other. There are different definitions of when this is so and according to Kaviany and Singh [2] the necessary condition is somewhere around $C/\lambda > 0.3$ and $C/\lambda > 0.5$ or even larger, with C being the average particle clearance.

Also attempts to numerically solve the radiation transfer equation (2.3) for porous media have been made by using *two-flux-* or *Schuster-Schwarzchild approximation* and *discrete ordinates methods*, some of these are talked about by Kaviany and Singh [2], who also introduce a *dependence-included discrete-ordinates method* to deal with dependent scattering. The two-flux models are simpler and neglect anisotropic effects.

2.1.2 Ray tracing Monte Carlo

Another way to look at radiative transfer in porous media is to try to predict the materials' attributes by directly simulating their structure. This involves creating some kind of reasonable model for the structure, for example a randomly packed bed of semitransparent spheres. Also the absorptivity and the refractive index of the material the system is made out of are needed.

Rays are then sent from randomly varied directions from one end of the system to the

other, using ray optics to calculate probabilities for how they are scattered and absorbed by the structure. The numbers of rays scattered and absorbed are recorded together with the distances they managed to travel without change. Also the number of rays that pass through the system and that end up in the same end of the system they started from are recorded, these give the transmission and the reflection properties of the material. A paper by Petrasch et al. [16] is a good example of this method.

2.1.3 Electromagnetic Wave Simulation

Another possible non-continuum approach to electromagnetic radiation in a porous dielectric medium is to simply calculate what happens to electromagnetic waves that enter it. This can be done by solving the volume integral equation, as presented by Tsang et al. [6]

$$\bar{E}(\bar{r}) = \bar{E}^{inc}(\bar{r}) + k^2 \int \mathrm{d}\bar{r}' \bar{\bar{G}}(\bar{r}, \bar{r}') \cdot (\epsilon_r(\bar{r}') - 1)\bar{E}(\bar{r}') \quad , \tag{2.10}$$

in a structure given with the help of relative permittivity

$$\epsilon_r(\bar{r}) = \begin{cases} \epsilon(\bar{r})/\epsilon_0 & \text{if } \bar{r} \in V_{solid} \\ 1 & \text{if } \bar{r} \in V_{empty} \end{cases} \tag{2.11}$$

Also in Eq. (2.10) $\bar{E}$ is the electric field, k the wavenumber and $\bar{\bar{G}}(\bar{r}, \bar{r}')$ the dyadic Green's function. The volume integral equation can be easily derived from Maxwell's laws as will be shown in the following section. It's solution can be used to get the electric field far away from the system, which in turn gives the information of how much of the original wave was absorbed, transmitted and reflected.

Solving Eq. (2.10) can only be done numerically and demands some computational power. Among the ways to numerically solve the Maxwell's equations in cases involving scattering of electromagnetic radiation are *the method of moments*, *the T-matrix method* and *the discrete dipole approximation*, also known as DDA. Of these the method of moments leads to a full matrix equation of order N and the number of operations needed for its solution is N^3 [6]. This may become very inconvenient for large systems.

2.2 The Discrete Dipole Approximation

Interestingly, the discrete dipole approximation was first developed by Purcell and Pennypacker [22] to study polarization of light by interstellar dust grains, however it is much more versatile than that and can be applied to many different kinds of scattering problems. The basic idea behind the discrete dipole approximation is that the structure that

is being simulated is approximated as consisting of finite size polarizable cubes or other shapes, which are polarized into dipoles by the incoming electromagnetic plane wave. The reflectance, absorbance and transmittance of the structure are then calculated based on the combination of fields of these dipoles and the field of the incoming wave far away from the structure. It is possible to model periodic structures consisting of dipoles, where a single target unit cell is repeated to create a plane. Fig. 2.1 is an example of what such a target unit cell could look like.

2.2.1 The Volume Integral Equation

As mentioned earlier, the volume integral equation (2.10) is derived form the Maxwell's equations, specifically the Maxwell-Faraday equation

$$\nabla \times \bar{E} = -\frac{\partial \bar{B}}{\partial t} \tag{2.12}$$

and Ampère's circuital law with Maxwell's correction

$$\nabla \times \bar{H} = \bar{J} + \frac{\partial \bar{D}}{\partial t}. \tag{2.13}$$

Now, if the scattered electric and magnetic fields $\bar{E}$ and $\bar{H}$ are assumed to be sinusoidal with frequency ω and $\bar{J} = 0$ because the system is dielectric, then Eqs. (2.12) and (2.13) become

$$\nabla \times \bar{E} = i\omega\bar{B} = i\omega\mu\bar{H} \tag{2.14}$$

and

$$\nabla \times \bar{H} = -i\omega\bar{D} = -i\omega\epsilon(\bar{r})\bar{E} \tag{2.15}$$

respectively. It is assumed that the permeability μ of the system does not differ significantly from the permiability of free space μ_0. Next, taking the curl of Eq. (2.14) and substituting Eq. (2.15) on the right side yields

$$\begin{aligned} \nabla \times \nabla \times \bar{E} &= -\omega^2\mu_0\epsilon(\bar{r})\bar{E} \\ \nabla \times \nabla \times \bar{E} - \omega^2\mu_0\epsilon_0\bar{E} &= \omega^2\mu_0\epsilon_0(\epsilon(\bar{r})/\epsilon_0 - 1)\bar{E} \\ \nabla \times \nabla \times \bar{E} - k^2\bar{E} &= k^2(\epsilon_r(\bar{r}) - 1)\bar{E}, \end{aligned} \tag{2.16}$$

because $\epsilon_r(\bar{r}) = \epsilon(\bar{r})/\epsilon_0$ and $k = \omega\sqrt{\epsilon_0\mu_0}$. The resulting equation for the scattered electric field, Eq. (2.16) is now in a fortunate form for which the solution is known [7] to be

$$\bar{E}_s(\bar{r}) = \int \mathrm{d}\bar{r}'\bar{\bar{G}}(\bar{r},\bar{r}') \cdot (\epsilon_r(\bar{r}') - 1)\bar{E}(\bar{r}'). \tag{2.17}$$

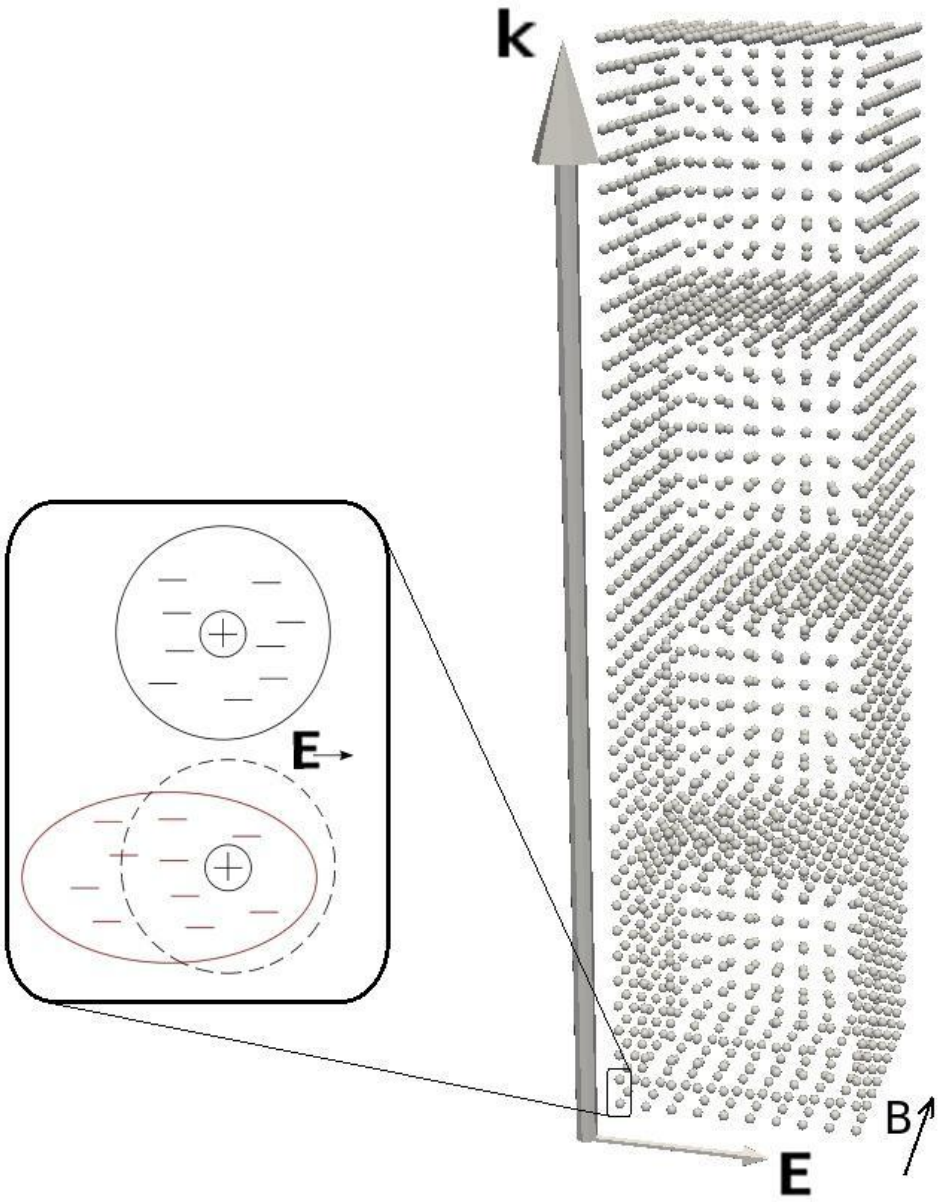

Figure 2.1: An example of a target unit cell made up of dipoles. **k** is the wave vector of the incoming plane wave. The zoomed in part shows how the electric field **E** of the incoming wave polarizes the dipoles. The unit cell in the picture has four cube shaped cavities. The walls between the cavities are two dipoles thick. Note that this exact structure was not used in the simulations, the structures that were used were bigger and had a larger number of dipoles.

The solution is given in terms of the dyadic Green's function $\bar{\bar{G}}(\bar{r},\bar{r}')$, which satisfies the following equation

$$\nabla \times \nabla \times \bar{\bar{G}}(\bar{r},\bar{r}') - k_0^2 \bar{\bar{G}}(\bar{r},\bar{r}') = \bar{\bar{I}}\delta(\bar{r}-\bar{r}'). \tag{2.18}$$

This can be easily confirmed by substituting $\bar{E}_s$ given by Eq. (2.17) to Eq. (2.16). In the definition (2.18) $\bar{\bar{I}}$ is the unit dyad, $\delta(\bar{r}-\bar{r}')$ the Dirac delta function and k_0 a constant. $\bar{\bar{G}}(\bar{r},\bar{r}')$ itself can be written in terms of Poisson's equation's Green's function $g(\bar{r},\bar{r}')$

$$\bar{\bar{G}}(\bar{r},\bar{r}') = (\bar{\bar{I}} + \frac{1}{k_0^2}\nabla\nabla)g(\bar{r},\bar{r}') \tag{2.19}$$

or in matrix form

$$\bar{\bar{G}}(\bar{r},\bar{r}') = \begin{pmatrix} k_0^2 + \frac{\partial^2}{\partial x'^2} & \frac{\partial^2}{\partial x'\partial y'} & \frac{\partial^2}{\partial x'\partial z'} \\ \frac{\partial^2}{\partial y'\partial x'} & k_0^2 + \frac{\partial^2}{\partial y'^2} & \frac{\partial^2}{\partial y'\partial z'} \\ \frac{\partial^2}{\partial z'\partial x'} & \frac{\partial^2}{\partial z'\partial y'} & k_0^2 + \frac{\partial^2}{\partial z'^2} \end{pmatrix} \frac{1}{k_0^2} g(\bar{r},\bar{r}'), \tag{2.20}$$

where

$$g(\bar{r},\bar{r}') = \frac{e^{ik_0|\bar{r}-\bar{r}'|}}{4\pi|\bar{r}-\bar{r}'|}. \tag{2.21}$$

However, looking at Eqs. (2.19) and (2.21) one can see that the dyadic Green's function has a singularity at $\bar{r} = \bar{r}'$. Quantitatively, in the case of a dielectric, the singularity can be interpreted as a point-like polarization charge caused by the external electric field $\bar{E}_{inc}$. Following Tsang et al. [6] this singularity can be dealt with by using the Cauchy principal value and writing $\bar{\bar{G}}$ as

$$\bar{\bar{G}}(\bar{r},\bar{r}') = PV\bar{\bar{G}}(\bar{r},\bar{r}') - \frac{\bar{\bar{L}}\delta(\bar{r}-\bar{r}')}{k^2}, \tag{2.22}$$

where PV signals that a small volume V_δ in which the singularity exists has been excluded and $\frac{\bar{\bar{L}}\delta(\bar{r}-\bar{r}')}{k^2}$ is the term that has been added to account for that volume. The dyad $\bar{\bar{L}}$ depends on the shape of the excluded volume V_δ and in the special case of the volume being a cube $\bar{\bar{L}} = \frac{\bar{\bar{I}}}{3}$.

The solution (2.17) for the scattered field still has the integral and that is why numerical methods are needed. The form of the volume integral equation on Eq. (2.10) is achieved by dividing the field $\bar{E}(\bar{r})$ into two scattered and incoming fields $\bar{E} = \bar{E}_{inc} + \bar{E}_s$ and then substituting Eq. (2.17).

2.2.2 The Dipole approximation

Now taking into account the singularity in the dyadic Green's function as in Eq. (2.22) and assuming that the excluded volume V_δ is the shape of a cube, the volume integral equation (2.10) becomes

$$\begin{aligned}\bar{E}(\bar{r}) =& \bar{E}_{inc}(\bar{r}) + k^2 \int_{V-V_\delta} \mathrm{d}\bar{r}' \bar{\bar{G}}(\bar{r},\bar{r}') \cdot (\epsilon_r(\bar{r}') - 1)\bar{E}(\bar{r}') \\ & - \frac{(\epsilon_r(\bar{r}) - 1)}{3} \bar{\bar{I}} \cdot \bar{E}(\bar{r}).\end{aligned} \tag{2.23}$$

At this point the Eq. (2.23) still describes the situation accurately in the sense of classical electrodynamics. The next step is to discretize the space, so that the continuous space becomes a discrete collection of small, but finite sized cubes, that are either empty, with $\epsilon_r = 1$, or filled with a dielectric so that $\epsilon_r \neq 1$.

$$\begin{aligned}\bar{E}(\bar{r}_i) =& \bar{E}_{inc}(\bar{r}_i) + k_0^2 \sum_{i=1}^{N} \sum_{j\neq i}^{N} \bar{\bar{G}}(\bar{r}_i,\bar{r}_j) \cdot \bar{E}(\bar{r}_j)(\epsilon_r(\bar{r}_j) - 1)\Delta V_j \\ & - \frac{(\epsilon_r(\bar{r}_i) - 1)}{3} \bar{\bar{I}} \cdot \bar{E}(\bar{r}_i)\end{aligned} \tag{2.24}$$

By marking $\bar{\bar{A}}_{ij} = -\frac{k_0^2}{\epsilon_0}\bar{\bar{G}}(\bar{r}_i,\bar{r}_j)$ and $\bar{p}_j = (\epsilon(\bar{r}_j) - \epsilon_0)\bar{E}(\bar{r}_j)\Delta V_j$, which is the dipole moment of the jth cube, this can be simplified to

$$\bar{E}_i = \bar{E}_i^{inc} - \sum_{i=1}^{N} \sum_{j\neq i}^{N} \bar{\bar{A}}_{ij} \cdot \bar{p}_j - \frac{(\epsilon_r(\bar{r}_i) - 1)}{3} \bar{E}_i, \tag{2.25}$$

or eliminating $\bar{E}_i$ altogether in favour of $\bar{p}_i$ and giving rise to the Clausius-Mossoti polarizability α_i

$$\begin{aligned}\bar{p}_i &= 3\epsilon_0 \Delta V \frac{\epsilon_r - 1}{\epsilon_r + 2} \left[\bar{E}_i^{inc} - \sum_{i=1}^{N} \sum_{j\neq i}^{N} \bar{\bar{A}}_{ij} \cdot \bar{p}_j \right] \\ &= \alpha_i \bar{E}_i^{inc} - \alpha_i \sum_{i=1}^{N} \sum_{j\neq i}^{N} \bar{\bar{A}}_{ij} \cdot \bar{p}_j.\end{aligned} \tag{2.26}$$

The Clausius-Mossoti polarizability α_i

$$\alpha_i = 3\epsilon_0 \Delta V \frac{\epsilon_r - 1}{\epsilon_r + 2}, \tag{2.27}$$

however is problematic, because it only works at the limit of long wavelength, and so other polarizabilities with finite wavelength corrections, that take into account the finite size of the dipoles, are often used in practice. For example, in this thesis a polarizability derived from a lattice dispersion relation by Gutkowicz-Krusin and Draine [9] is used.

2.2.3 Lattice dispersion relation and polarizabilities

On this subsection, first the lattice dispersion relation and then the polarizabilities that are used are derived following Gutkowicz-Krusin and Draine [9]. To start deriving the lattice dispersion relation, we first assume an infinite rectangular lattice, where the lattice sites are $\mathbf{x}_n = (n_1 d_1, n_2 d_2, n_3 d_3)$. The n_i are integers and the d_i are the lattice constants. Now if there is an electric field $\mathbf{E}$ in the lattice, the polarization $\mathbf{P}$ is

$$\mathbf{P} = \alpha \cdot \mathbf{E}. \tag{2.28}$$

In this more general case, the polarizability α is a tensor. Because in this dielectric system the only currents are produced by changes in polarization $\mathbf{J} = \frac{\mathrm{d}\mathbf{P}}{\mathrm{d}t}$, and because charge needs to be conserved $\nabla \cdot \mathbf{J} = 0$, it follows that

$$\nabla \cdot \mathbf{P} = 0. \tag{2.29}$$

It is also assumed that the electric field that is polarizing the lattice takes the form of a plane wave, as before, and that on lattice site $\mathbf{x}_n$ the polarization consequently takes a similar form

$$\mathbf{P}_n(t) = \mathbf{P}_0 e^{i(\mathbf{k}\cdot\mathbf{x}_n - \omega t)}. \tag{2.30}$$

From this it follows that the current in the lattice looks like

$$\mathbf{J} = -i\omega \sum_n \mathbf{P}_n(t)\delta^3(\mathbf{x} - \mathbf{x}_n). \tag{2.31}$$

Next, Lorentz gauge condition

$$\nabla \cdot \mathbf{A} + \frac{1}{c}\frac{\partial \varphi}{\partial t} = 0 \tag{2.32}$$

is used to derive a wave equation. $\mathbf{A}$ is the magnetic vector potential $\mathbf{B} = \nabla \times \mathbf{A}$ and φ is electric potential $\mathbf{E} = \nabla\varphi$. To start deriving the wave equation we look again at

Ampere's circuital law (2.13).

$$\begin{aligned}
\nabla \times \mathbf{B} &= \mu_0 \mathbf{J} + \frac{1}{c^2}\frac{\partial \mathbf{E}}{\partial t} \\
\nabla \times (\nabla \times \mathbf{A}) &= \mu_0 \mathbf{J} + \frac{1}{c^2}\frac{\partial}{\partial t}(-\nabla\varphi - \frac{\partial \mathbf{A}}{\partial t}) \\
\nabla(\nabla \cdot \mathbf{A}) - \nabla^2 \mathbf{A} &= \mu_0 \mathbf{J} - \frac{1}{c^2}\nabla\frac{\partial \varphi}{\partial t} - \frac{1}{c^2}\frac{\partial^2 \mathbf{A}}{\partial t^2} \\
\nabla\left(\nabla \cdot \mathbf{A} + \frac{1}{c^2}\frac{\partial \varphi}{\partial t}\right) &= \mu_0 \mathbf{J} + \nabla^2 \mathbf{A} - \frac{1}{c^2}\frac{\partial^2 \mathbf{A}}{\partial t^2} \\
0 &= -i\mu_0\omega \sum_n \mathbf{P}_n(t)\delta^3(\mathbf{x} - \mathbf{x}_n) + \nabla^2 \mathbf{A} + \frac{\omega^2}{c^2}\mathbf{A}
\end{aligned}$$

$$\nabla^2 \mathbf{A} + \frac{\omega^2}{c^2}\mathbf{A} = i\mu_0\omega \mathbf{P}_0 e^{i(\mathbf{k}\cdot\mathbf{x} - \omega t)} \sum_n \delta^3(\mathbf{x} - \mathbf{x}_n) \tag{2.33}$$

The final form, Eq. (2.33) is the wave equation that was needed.

Now it is necessary to solve $\mathbf{A}$. This is done by first expanding $\mathbf{A}$ into a series

$$\mathbf{A}(\mathbf{x}, t) = e^{i(\mathbf{k}\cdot\mathbf{x} - \omega t)} \sum_n \mathbf{a}_n e^{i(\mathbf{q}\cdot\mathbf{x})} \tag{2.34}$$

and then substituting it into the wave equation (2.33). The $\mathbf{q}$ in series (2.34) is simply the reciprocal lattice of the original lattice,

$$\mathbf{q} = 2\pi\left(\frac{n_1}{d_1}, \frac{n_2}{d_2}, \frac{n_3}{d_3}\right). \tag{2.35}$$

If also the identity

$$\sum_n \delta^3(\mathbf{x} - \mathbf{x}_n) = \frac{1}{d_1 d_2 d_3}\sum_n e^{i\mathbf{q}\cdot\mathbf{x}} \tag{2.36}$$

is used on the delta functions, then the $\mathbf{a}_n$ can be solved from the wave equation (2.33) to yield

$$\begin{aligned}
-(\mathbf{k} + \mathbf{q})^2 \sum_n \mathbf{a}_n e^{i\mathbf{q}\cdot\mathbf{x}} + \frac{\omega^2}{c^2}\sum_n \mathbf{a}_n e^{i\mathbf{q}\cdot\mathbf{x}} &= \frac{i\mu_0\omega}{d_1 d_2 d_3}\mathbf{P}_0 \sum_n e^{i\mathbf{q}\cdot\mathbf{x}} \\
\sum_n \mathbf{a}_n e^{i\mathbf{q}\cdot\mathbf{x}} &= \frac{i\mu_0\omega}{d_1 d_2 d_3}\mathbf{P}_0\left[\frac{\omega^2}{c^2} - (\mathbf{k} + \mathbf{q})^2\right]^{-1}\sum_n e^{i\mathbf{q}\cdot\mathbf{x}} \\
\mathbf{a}_n &= \frac{i\mu_0\omega}{d_1 d_2 d_3}\mathbf{P}_0\left[\frac{\omega^2}{c^2} - (\mathbf{k} + \mathbf{q})^2\right]^{-1}
\end{aligned} \tag{2.37}$$

In order solve Eq. (2.37) further it is useful to consider the effect of all of the other lattice sites on one specific lattice site.

$$\begin{aligned}\mathbf{E}_{other}(\mathbf{x},t) &= -\nabla\varphi_{other} - \frac{\partial \mathbf{A}_{other}}{\partial t} \\ &= \nabla\left(\frac{ic^2}{\omega}\nabla\cdot\mathbf{A}_{other}\right) + i\omega\mathbf{A}_{other}\end{aligned} \tag{2.38}$$

This can be used to describe polarization as in Eq. (2.28) and so $\mathbf{a}_n$ in Eq. (2.37) can be expressed in terms of polarizability as

$$\mathbf{a}_n = \frac{i\mu_0\omega}{d_1d_2d_3}\alpha\cdot\mathbf{E}_{other}(0,0)\left[\frac{\omega^2}{c^2} - (\mathbf{k}+\mathbf{q})^2\right]^{-1} \tag{2.39}$$

The vector potential due to a single dipole at the origin is given by Gutkowicz-Krusin and Draine [9] as

$$\begin{aligned}\mathbf{A}_{self} &= -\frac{i\omega}{c}\frac{\sqrt{\mu_0}}{4\pi\sqrt{\epsilon_0}}\mathbf{P}_0\frac{e^{i\omega r/c}}{r} \\ &= -\frac{i\omega}{c}\frac{\sqrt{\mu_0}}{4\pi\sqrt{\epsilon_0}}\alpha\cdot\mathbf{E}_{other}(0,0)\frac{e^{i\omega r/c}}{r}e^{-i\omega t}.\end{aligned} \tag{2.40}$$

If another identity

$$\frac{e^{i\omega r/c}}{r} = \frac{e^{i\mathbf{k}\cdot\mathbf{x}}}{2\pi^2}\int \mathrm{d}^3k'\frac{e^{i\mathbf{k}'\cdot\mathbf{x}}}{|\mathbf{k}'+\mathbf{k}|^2-\omega^2/c^2} \tag{2.41}$$

is used together with $\mathbf{A}_{self}$, then $\mathbf{A}_{other}$ can be expressed as

$$\begin{aligned}\mathbf{A}_{other} =& \mathbf{A} - \mathbf{A}_{self} \\ =& \frac{i\mu_0\omega e^{i\mathbf{k}\cdot\mathbf{x}-i\omega t}}{d_1d_2d_3}\alpha\cdot\mathbf{E}_{other}(0,0)\left[\sum_n \frac{e^{i\mathbf{q}\cdot\mathbf{x}}}{\frac{\omega^2}{c^2}-(\mathbf{k}+\mathbf{q})^2}\right. \\ &\left. + \frac{d_1d_2d_3}{8\pi^3}\int \mathrm{d}^3k'\frac{e^{i\mathbf{k}'\cdot\mathbf{x}}}{|\mathbf{k}'+\mathbf{k}|^2-\omega^2/c^2}\right]\end{aligned} \tag{2.42}$$

This, in turn allows $\mathbf{E}_{other}$ to be solved by substituting $\mathbf{A}_{other}$ from Eq. (2.42) into Eq. (2.38).

$$\begin{aligned}E_{other,i}(\mathbf{x},t) = -\frac{c^2\mu_0}{d_1d_2d_3}\sum_{j=1}^{3}\sum_{l=1}^{3}&\left[\sum_{\mathbf{n}}\left(\tfrac{\omega^2}{c^2}\delta_{il}-(k_i+q_i)(k_l+q_l)\right)\frac{e^{i(\mathbf{k}+\mathbf{q})\cdot\mathbf{x}}}{|\mathbf{k}+\mathbf{q}|^2-\frac{\omega^2}{c^2}}\right. \\ &\left. - \frac{d_1d_2d_3}{8\pi^3}\int \mathrm{d}^3k'\left(\tfrac{\omega^2}{c^2}\delta_{il}-(k_i+k_i')(k_l+k_l')\right)\frac{e^{i(\mathbf{k}+\mathbf{k}')\cdot\mathbf{x}}}{|\mathbf{k}+\mathbf{k}'|^2-\frac{\omega^2}{c^2}}\right]e^{-i\omega t}\alpha_{lj}E_{other,j}(0,0)\end{aligned} \tag{2.43}$$

Now Eq. (2.43) can be used to solve the polarizability α, if the dispersion relation is known. To make things easier, when $\mathbf{x} = 0$ and $t = 0$ Eq. (2.43) can be written in a shorter way

$$\sum_{j=1}^{3}\sum_{l=1}^{3} M_{il}\alpha_{lj}E_{other,j} = E_{other,i} \tag{2.44}$$

or, if divided by E,

$$\sum_{j=1}^{3}\sum_{l=1}^{3} M_{il}\alpha_{lj}e_j = e_i, \tag{2.45}$$

where M_{il} is

$$M_{il} = -\frac{c^2\mu_0}{d_1d_2d_3}\left[\sum_{\mathbf{n}} \frac{\frac{\omega^2}{c^2}\delta_{il} - (k_i+q_i)(k_l+q_l)}{|\mathbf{k}+\mathbf{q}|^2 - \frac{\omega^2}{c^2}} - \frac{d_1d_2d_3}{8\pi^3}\int \mathrm{d}^3k' \frac{\frac{\omega^2}{c^2}\delta_{il} - (k_i+k'_i)(k_l+k'_l)}{|\mathbf{k}+\mathbf{k}'|^2 - \frac{\omega^2}{c^2}}\right]. \tag{2.46}$$

The dispersion relation that is used to derive the α_{lj} is

$$\mathbf{k} = \frac{m\omega}{c}\hat{\mathbf{k}}, \tag{2.47}$$

where m is the refractive index of the material. Another condition that must be fulfilled is

$$\mathbf{k}\cdot\mathbf{P}_0(0) = 0 \tag{2.48}$$

or, written in a more open way

$$\sum_{j=1}^{3}\sum_{l=1}^{3} k_l\alpha_{lj}e_j = 0, \tag{2.49}$$

which follows from how the polarization must be a reaction to the electric field. The e_j are the components of a unit vector that is parallel to the electric field. Next Gutkowicz-Krusin and Draine [9] divide the M_{ij} into two parts

$$M_{ij} = M_{ij}^C + T_{ij}. \tag{2.50}$$

Here M_{ij}^C are the matrix elements for cubic lattice that had been solved in an earlier paper by Draine and Goodman [23]. The T_{ij} on the other hand are the matrix elements for a rectangular lattice.

Next step is to approximate and ignore terms that of the order of ν^4, with $\nu = \frac{\omega(d_1 d_2 d_3)^{1/3}}{2\pi c}$.

$$\alpha_{ij} = \alpha_{ij}^{(0)} + \alpha_{ij}^{(1)} + O(\nu^4) \tag{2.51}$$

$$M_{ij}^C = M_{ij}^{C(0)} + M_{ij}^{C(1)} + O(\nu^4) \tag{2.52}$$

$$T_{ij} = T_{ij}^{(0)} + T_{ij}^{(1)} + O(\nu^4) \tag{2.53}$$

$$e_i = e_i^{(0)} + e_i^{(1)} + O(\nu^4) \tag{2.54}$$

The terms with the superscript (0) are the zeroth order approximation, they give the exact result if $\lambda >> d_i$. The terms with the superscript (1) are the corrections to the first long wavelength limit approximation. It is also practical to use dimensionless variables

$$\tilde{q} = \frac{2\pi}{(d_1 d_2 d_3)^{1/3}} \tag{2.55}$$

$$\nu = \frac{\omega}{c\tilde{q}} \tag{2.56}$$

$$\bar{\beta} = \frac{\mathbf{k}}{\tilde{q}} \tag{2.57}$$

$$\mathbf{Q} = \frac{\mathbf{q}}{\tilde{q}} \tag{2.58}$$

$$\gamma = -\frac{c^2 \mu_0}{d_1 d_2 d_3}\alpha. \tag{2.59}$$

Using these, Eq. (2.46) can be written

$$M_{il} = \sum_{\mathbf{n}} \frac{\nu^2 \delta_{il} - (\beta_i + Q_i)(\beta_l + Q_l)}{|\bar{\beta} + \mathbf{Q}|^2 - \nu^2} - \int \mathrm{d}^3\beta' \frac{\nu^2 \delta_{il} - (\beta_i + \beta_i')(\beta_l + \beta_l')}{|\bar{\beta} + \bar{\beta}'|^2 - \nu^2}. \tag{2.60}$$

The terms $M_{ij}^{C(0)}$ from Eq. (2.52) can be written

$$M_{ij}^{C(0)} = \frac{m^2 + 2}{3(m^2 - 1)}\delta_{ij} - \frac{m^2}{m^2 - 1}\frac{k_i k_j}{k^2}. \tag{2.61}$$

The $\frac{k_i}{k}$ are components of the unit vector $\hat{\mathbf{k}}$. Instructions on how to get $M_{ij}^{C(0)}$ and $M_{ij}^{C(1)}$

$$M_{ij}^{C(1)} = \nu^2 \delta_{ij}[c_1 + m^2 c_2(1 - 3a_i^2)] + m^2 \nu^2 (1 - \delta_{ij}) c_3 a_i a_j - \frac{4\pi^2 i}{3}\delta_{ij}\nu^3 \tag{2.62}$$

can be found in the appendices of [23]. The constants c_1, c_2 and c_3 are

$$c_1 = -5.9424219... \tag{2.63}$$

$$c_2 = 0.5178819... \tag{2.64}$$

$$c_3 = 4.0069747... \quad . \tag{2.65}$$

For the rectangular lattice part

$$T_{ij}^{(0)} = \delta_{ij}\left[\sum_{\mathbf{n}} \frac{n_i^2}{|\mathbf{n}|^2} - \sum_{\mathbf{n}} \frac{Q_i^2}{|\mathbf{Q}|^2}\right] \tag{2.66}$$

and

$$\begin{aligned} T_{ij}^{(1)} = m^2\nu^2 e_i e_j \Bigg[& \sum_{\mathbf{n}} \frac{1}{|\mathbf{n}|^2} - \sum_{\mathbf{n}} \frac{1}{|\mathbf{Q}|^2} - 2\left(\sum_{\mathbf{n}} \frac{n_i^2}{|\mathbf{n}|^4} - \sum_{\mathbf{n}} \frac{Q_i^2}{|\mathbf{Q}|^4}\right) \\ & - 2\left(\sum_{\mathbf{n}} \frac{n_j^2}{|\mathbf{n}|^4} - \sum_{\mathbf{n}} \frac{Q_j^2}{|\mathbf{Q}|^4}\right) + 8\left(\sum_{\mathbf{n}} \frac{n_i^2 n_j^2}{|\mathbf{n}|^6} - \sum_{\mathbf{n}} \frac{Q_i^2 Q_j^2}{|\mathbf{Q}|^6}\right)\Bigg] \\ & - \nu^2\delta_{ij}\Bigg[\sum_{\mathbf{n}} \frac{1}{|\mathbf{n}|^2} - \sum_{\mathbf{n}} \frac{1}{|\mathbf{Q}|^2} + (m^2-1)\left(\sum_{\mathbf{n}} \frac{n_i^2}{|\mathbf{n}|^4} - \sum_{\mathbf{n}} \frac{Q_i^2}{|\mathbf{Q}|^4}\right) \\ & + 8m^2 e_i^2\left(\sum_{\mathbf{n}} \frac{n_i^4}{|\mathbf{n}|^6} - \sum_{\mathbf{n}} \frac{Q_i^4}{|\mathbf{Q}|^6}\right) - 4m^2\sum_{l=1}^{3} e_l^2\left(\sum_{\mathbf{n}} \frac{n_i^2 n_l^2}{|\mathbf{n}|^6} - \sum_{\mathbf{n}} \frac{Q_i^2 Q_l^2}{|\mathbf{Q}|^6}\right)\Bigg]. \end{aligned} \tag{2.67}$$

Again, the math for deriving $T_{ij}^{(0)}$ and $T_{ij}^{(1)}$ can be found in the appendix of [9].

Now that $M_{ij}^{(0)} = M_{ij}^{C(0)} + T_{ij}^{(0)}$ is known, it can be used together with Equations (2.45) and (2.49) to solve $\gamma^{(0)}$, which needs to be diagonal in order to reduce to the Clausius-Mossoti polarizability for cubic lattices.

$$\gamma_{ii}^{(0)} = \frac{3(m^2-1)}{m^2+2}\left[1 + \frac{3(m^2-1)}{(m^2+2)}\left(\sum_{\mathbf{n}} \frac{n_i^2}{|\mathbf{n}|^2} - \sum_{\mathbf{n}} \frac{Q_i^2}{|\mathbf{Q}|^2}\right)\right]^{-1} \tag{2.68}$$

Since $\frac{Q_i^2}{|\mathbf{Q}|^2} = \frac{n_i^2}{|\mathbf{n}|^2}$ when $d_1 = d_2 = d_3$, Eq. (2.68) is compatible with the Clausius-Mossoti polarizability (2.27).

Solving the finite wavelength corrections for polarizability is now reasonably straightforward. Following how the $\gamma_{ij}^{(0)}$ were solved, Eq. (2.45) is written with the corrections.

$$\sum_{j=1}^{3}\sum_{l=1}^{3}(M_{il}^{(0)} + M_{il}^{(1)})(\gamma_{lj}^{(0)} + \gamma_{lj}^{(1)})(e_j^{(0)} + e_j^{(1)}) = e_i^{(0)} + e_i^{(1)} \tag{2.69}$$

Because the corrections are assumed to be small, any resulting terms with more than one correction, such as $M_{il}^{(0)}\gamma_{lj}^{(1)}e_j^{(1)}$, are neglected. This results in

$$\sum_{j=1}^{3}\sum_{l=1}^{3} M_{il}^{(1)}\gamma_{lj}^{(0)}e_j^{(0)} + \sum_{j=1}^{3}\sum_{l=1}^{3} M_{il}^{(0)}\left[\gamma_{lj}^{(1)}e_j^{(0)} + \gamma_{lj}^{(0)}e_j^{(1)}\right] = e_i^{(1)}. \tag{2.70}$$

The same can be done to condition (2.49) to yield

$$\sum_{i=1}^{3}\sum_{j=1}^{3} \frac{k_i}{k}\left[\gamma_{ij}^{(0)}e_j^{(1)} + \gamma_{ij}^{(1)}e_j^{(0)}\right] = 0. \tag{2.71}$$

The next step is to use $M_{il}^{(0)}$, which was solved before, Eq. (2.45) at the long wavelength limit and the condition (2.71), to render the second term of Eq. (2.70) into a more useful form.

$$\begin{aligned}\sum_{j=1}^{3}\sum_{l=1}^{3} M_{il}^{(0)}\left[\gamma_{lj}^{(1)}e_j^{(0)} + \gamma_{lj}^{(0)}e_j^{(1)}\right] &= \sum_{j=1}^{3}\left(\tfrac{m^2+2}{3(m^2-1)} + \sum_{\mathbf{n}}\tfrac{n_i^2}{|\mathbf{n}|^2} - \sum_{\mathbf{n}}\tfrac{Q_i^2}{|\mathbf{Q}|^2}\right)\left[\gamma_{ij}^{(1)}e_j^{(0)} + \gamma_{ij}^{(0)}e_j^{(1)}\right] \\ &= \sum_{j=1}^{3}\left[\frac{\gamma_{ij}^{(1)}}{\gamma_{ii}^{(0)}}e_j^{(0)}\right] + e_i^{(1)}\end{aligned} \tag{2.72}$$

This change simplifies Eq. (2.70) into

$$\sum_{j=1}^{3}\left[\frac{\gamma_{ij}^{(1)}}{\gamma_{ii}^{(0)}} + M_{ij}^{(1)}\gamma_{jj}^{(0)}\right]e_j^{(0)} = 0. \tag{2.73}$$

It is clear to see that the Eq. (2.73) is solved if

$$\gamma_{ij}^{(1)} = \gamma_{ii}^{(0)}\gamma_{jj}^{(0)}M_{ij}^{(1)}, \tag{2.74}$$

Which gives us the finite wavelength correction to polarizability. It is worth noting that this solution is not unique and according to Gutkowicz-Krusin and Draine [9] some other solution could offer more convenience, depending on usage.

2.2.4 On the numerical methods

The two numerical methods that are used in DDA to solve Eq. (2.26) are the fast Fourier transform, or FFT, and the conjugate gradient method. Specifically, FFT is used for speeding up the calculation of the products

$$\sum_{i=1}^{N}\sum_{j\neq i}^{N} \bar{\bar{A}}_{ij}\cdot\bar{p}_j \tag{2.75}$$

and the conjugate gradient method is applied in solving the $\bar{p}_i$ from Eq. (2.26).

The use of conjugate gradient method is necessary, because given large enough matrix, using non-iterative methods, such as the Gauss-Jordan elimination method, becomes slow and inaccurate due to rounding errors.

2.2.5 Periodic structures

The discrete dipole approximation has been generalized for targets periodic in one or two dimensions by Draine and Flatau [8]. Following their approach the two dimensioned periodic target can be thought of as a plane of copies of a target unit cell. The dipoles that make up the original target unit cell, at lattice site $(0, 0)$, are at positions $\bar{r}_{j00}$, and the dipoles of a copy target unit cell at lattice site (m, n) are at positions

$$\bar{r}_{jmn} = \bar{r}_{j00} + m\bar{L}_y + n\bar{L}_z. \tag{2.76}$$

m and n are integers and the vectors $\bar{L}_y$ and $\bar{L}_z$ are the target unit cells lengths in y- and z-directions. y- and z-directions are on the plane with the target units and the x axis is perpendicular to that plane.

The polarization of the original target unit cell $\bar{p}_{j00}$ is the same as before in Eq. (2.26) and the polarizations of its copies are simply phase shifted

$$\bar{p}_{jmn} = \bar{p}_{j00} e^{i(m\bar{k}_0 \cdot \bar{L}_y + n\bar{k}_0 \cdot \bar{L}_z)}. \tag{2.77}$$

This is possible, because the polarization must have similar time and place dependencies as the incoming electric field $\bar{E}_{inc}$, which creates it.

In Eq. (2.25) $-\bar{\bar{A}}_{ij} \cdot \bar{p}_j$ gave the electric field of dipole j at $\bar{r}_i$. This can be easily generalized to $-\bar{\bar{A}}_{i,jmn} \cdot \bar{p}_{jmn}$, which gives the electric field of dipole jmn at $\bar{r}_{i00}$. Now, by making phase shifts as in Eq. (2.77), an $\tilde{A}$ such that $\tilde{A}_{ij} \cdot \bar{p}_{j00}$ gives the part of the electric field at $\bar{r}_{i00}$ caused by dipole $j00$ and its copies jmn, can be written

$$\tilde{A}_{ij} = \sum_{m=-\infty}^{\infty} \sum_{n=-\infty}^{\infty} (1 - \delta_{ij}\delta_{m0}\delta_{n0}) \bar{\bar{A}}_{i,jmn} e^{i(m\bar{k}_0 \cdot \bar{L}_y + n\bar{k}_0 \cdot \bar{L}_z)}. \tag{2.78}$$

In this thesis, as in the paper by Draine and Flatau [8], the sums in Eq. (2.78) are suppressed at large $r_{i,jmn}$ with the addition of a factor $e^{-(\gamma k_0 r_{i,jmn})^4}$. This is done to speed up the calculation, and the constant γ determines how quickly the sums are suppressed.

The final form of the equation, which is solved in DDA for periodic targets, is

$$\bar{p}_{i00} = \alpha_i \left[\bar{E}_{inc}(\bar{r}_i) - \sum_{j \neq i} \tilde{A}_{ij} \cdot \bar{p}_{j00} e^{-(\gamma k_0 r_{i,jmn})^4} \right]. \tag{2.79}$$

2.2.6 From Polarizations to Scattering

To get useful information about scattering from the polarizations, it is necessary to calculate the scattered electric field far away from the target. The necessary condition, for being far enough away from the target to ignore near field effects, is $kr \gg 1$.

At this distance the electric field caused by the dipole jmn is

$$\bar{E}_{jmn} = \frac{k_0^2 e^{ik_0|\bar{r}-\bar{r}_{jmn}|}}{|\bar{r}-\bar{r}_{jmn}|}\left[\bar{\bar{I}} - \frac{(\bar{r}-\bar{r}_{jmn})(\bar{r}-\bar{r}_{jmn})}{|\bar{r}-\bar{r}_{jmn}|^2}\bar{p}_{jmn}\right] \tag{2.80}$$

According to Draine and Flatau [8], the field at $\bar{r} = r\hat{k}_s$ is mostly affected by the dipoles that lie in an area called the Fresnel zone, which has the radius $R_F \approx \sqrt{\frac{r}{k_0}}$. The $\hat{k}_s$ is a unit vector which is parallel to the wave vector of scattered radiation $\bar{k}_s = k_0\hat{k}_s$, in other words it is the direction of the scattered radiation. If dipoles that are not in the Fresnel zone are neglected, the scattered field becomes

$$\begin{aligned}\bar{E}_s(\bar{r}) \approx& \frac{k_0^2}{r}\left[1-\hat{k}_s\hat{k}_s\right]\sum_{j,m,n} e^{ik_0|\bar{r}-\bar{r}_{jmn}|}\bar{p}_{jmn} \\ =& \frac{k_0^2}{r}\left[1-\hat{k}_s\hat{k}_s\right]\sum_{j}\bar{p}_{j00}\sum_{m,n} e^{ik_0|\bar{r}-\bar{r}_{jmn}|+i(m\bar{k}_0\cdot\bar{L}_y+n\bar{k}_0\cdot\bar{L}_z)}.\end{aligned} \tag{2.81}$$

The $|\bar{r}-\bar{r}_{jmn}|$ in the exponent can be further written open and approximated using the binomial series $(1-x^2)^{1/2} = 1 - \frac{x^2}{2} - \frac{x^4}{8} - ...$ and Eq. (2.76).

$$\begin{aligned}|\bar{r}-\bar{r}_{jmn}| =& r\sqrt{1-2\frac{\bar{r}\cdot\bar{r}_{jmn}}{r^2}+\frac{r_{jmn}^2}{r^2}} \\ =& r\left(1-\frac{\bar{r}\cdot\bar{r}_{jmn}}{r^2}+\frac{r_{jmn}^2}{2r^2}-\frac{2^2(\bar{r}\cdot\bar{r}_{jmn})^2}{8r^4}+...\right) \\ \approx& r-\hat{k}_s\cdot\bar{r}_{jmn}+\frac{r_{jmn}^2}{2r}-\frac{(\hat{k}_s\cdot\bar{r}_{jmn})^2}{2r} \\ =& r-\hat{k}_s\cdot\bar{r}_{j00}-m\hat{k}_s\cdot\bar{L}_y-n\hat{k}_s\cdot\bar{L}_z+\frac{1}{2r}[(\bar{r}_{j00}+m\bar{L}_y+n\bar{L}_z)^2 \\ & -(\hat{k}_s\cdot\bar{r}_{j00}+m\hat{k}_s\cdot\bar{L}_y+n\hat{k}_s\cdot\bar{L}_z)^2] \\ \approx& r-\hat{k}_s\cdot\bar{r}_{j00}-m\hat{k}_s\cdot\bar{L}_y-n\hat{k}_s\cdot\bar{L}_z+\frac{1}{2r}[m^2L_y^2+n^2L_z^2-m^2(\hat{k}_s\cdot\bar{L}_y)^2 \\ & -n^2(\hat{k}_s\cdot\bar{L}_z)^2+2mn\bar{L}_y\cdot\bar{L}_z+2mn(\hat{k}_s\cdot\bar{L}_y)(\hat{k}_s\cdot\bar{L}_z)]\end{aligned} \tag{2.82}$$

In the last step of (2.82) terms that are of the order of $\frac{mL}{r}$ have been neglected, because they approach 0 much faster than the others as r goes to infinity. The final form of Eq. (2.82) looks ugly, but is necessary in order to eliminate $\bar{r}_{jmn}$.

Now the electric field of Eq. (2.81) looks like

$$\bar{E}_s = \frac{e^{i\bar{k}_s\cdot\bar{r}-i\omega t}}{k_0 r}\bar{F}_{TUC}(\hat{k}_s)G(r,\bar{k}_s), \tag{2.83}$$

where

$$\bar{F}_{TUC} = k_0^3\left[\bar{\bar{I}} - \hat{k}_s\hat{k}_s\right]\sum_{j=1}^{N}\bar{p}_{j00}e^{i\omega t - i\bar{k}_s\cdot\bar{r}_{j00}}. \tag{2.84}$$

and

$$G(r,\bar{k}_s) = \sum_{m,n} e^{i\Big\{m(\bar{k}_0-\bar{k}_s)\cdot\bar{L}_y + n(\bar{k}_0-\bar{k}_s)\cdot\bar{L}_z + \frac{1}{2rk_0}\Big[m^2\left(k_0^2L_y^2-(\bar{k}_s\cdot\bar{L}_y)^2\right) + n^2\left(k_0^2L_z^2-(\bar{k}_s\cdot\bar{L}_z)^2\right) + 2mn\left(k_0^2\bar{L}_y\cdot\bar{L}_z-(\bar{k}_s\cdot\bar{L}_y)(\bar{k}_s\cdot\bar{L}_z)\right)\Big]\Big\}}. \tag{2.85}$$

The only difference from non-periodic DDA in Eq. (2.83) comes from the factor $G(r,\bar{k}_s)$. If $G = 1$, the scattered electric field reduces to that of one produced by a single target unit cell, instead of a plane consisting of them.

According to Draine and Flatau [8] $G(r,\bar{k}_s)$ sums up to 0 unless the requirement

$$\begin{aligned}(\bar{k}_s - \bar{k}_0)\cdot\bar{L}_y &= 2\pi M, \qquad M = 0,\pm1,\pm2,...\\ (\bar{k}_s - \bar{k}_0)\cdot\bar{L}_z &= 2\pi N, \qquad N = 0,\pm1,\pm2,...\end{aligned} \tag{2.86}$$

is met. In practice this means that the target plane acts as a diffraction grating with M and N giving the orders of diffraction of the reflected or transmitted wave, depending on the direction of $\bar{k}_s$. This is because two different scattered wave vectors can give rise to the same M or N, one $\bar{k}_s$ accounts for the transmitted and other for the reflected wave.

If Eqs. (2.86) apply, the $G(r,\bar{k}_s)$ from Eq. (2.85) can be further simplified by further following Draine and Flatau and treating the sum as an integral instead. Both of the

integrals are of a Gaussian function and so the solutions are known.

$$
\begin{aligned}
G(r,\bar{k}_s) \approx \lim_{\epsilon\to 0^+} \int_{-\infty}^{\infty} \mathrm{d}m \int_{-\infty}^{\infty} \mathrm{d}n\, e^{\frac{i(1+i\epsilon)}{2k_0 r}\Big[m^2\left(k_0^2L_y^2-(\bar{k}_s\cdot\bar{L}_y)^2\right)+n^2\left(k_0^2L_z^2-(\bar{k}_s\cdot\bar{L}_z)^2\right)} \\
e^{-2(\bar{k}_s\cdot\bar{L}_y)(\bar{k}_s\cdot\bar{L}_z)mn\Big]} \\
= \lim_{\epsilon\to 0^+} \frac{1}{L_yL_z} \int_{-\infty}^{\infty} \mathrm{d}y \int_{-\infty}^{\infty} \mathrm{d}z\, e^{\frac{i(1+i\epsilon)}{2k_0 r}\left[k_0^2(y^2+z^2)-\left(\frac{\bar{k}_s\cdot\bar{L}_y}{L_y}y+\frac{\bar{k}_s\cdot\bar{L}_z}{L_z}z\right)^2\right]} \\
= \frac{2\pi i r}{k_0L_yL_z\sqrt{k_0^2-(\bar{k}_s\cdot\bar{L}_y/L_y)^2-(\bar{k}_s\cdot\bar{L}_z/L_z)^2}} \\
= \frac{2\pi i r}{k_0L_yL_z\hat{x}\cdot\bar{k}_s} \qquad (2.87)
\end{aligned}
$$

It is worth noting that y and z are related to r_{jmn} and not r, which can be treated as a constant regarding the integrals. Finally when the simplified form from Eq. (2.87) is substituted into Eq. (2.83) the scattered electric field reduces to

$$\bar{E}_s = \frac{2\pi i e^{i\bar{k}_s\cdot\bar{r}-i\omega t}}{k_0L_yL_z\hat{x}\cdot\bar{k}_s}\bar{F}_{TUC}(\hat{k}_s). \qquad (2.88)$$

The scattered electric field can be used to construct 4x4 Mueller matrices, which in turn can be used to calculate the reflection and transmission coefficients, R and T, for the incoming wave that was used in the calculation. The use of Mueller matrices requires the incoming wave to be written as a Stokes vector. The Mueller matrix S gives the scattered wave's Stokes vector $\bar{I}_s$ when multiplied by the incoming wave $\bar{I}_{inc}$

$$\bar{I}_{sca,\alpha} = S\bar{I}_{inc,\beta}. \qquad (2.89)$$

α and β are the angles of the scattered and incoming vectors.

For the sake of simplicity and because of a problem with the code that was used in simulations, only the Stokes vector that corresponds to linearly polarized waves, $\bar{I}_{inc} = (1\ 1\ 0\ 0)^T$, is used in this thesis. The first element of the Stokes vector represents the waves intensity, and since only the relative intensities of the incoming and scattered waves are necessary for the calculation of the reflection, absorption and transmission coefficients, then only two elements of the Mueller matrix, S_{11} and S_{12}, are needed. Using the same definition as Bohren and Huffman [10], the second element is the difference between the intensities of the horizontal and vertical components of the wave. It can be thought of as a measure for how linearly polarized the wave is. The third element is a similar measure

for linear polarization, but this time at 45 deg angle from before. The fourth element measures how circularly polarized the wave is.

The elements of the Mueller matrix S_{ij} can be calculated from the elements of the scattering amplitude matrix S_i. For example

$$S_{11} = \tfrac{1}{2}\left(|S_1|^2 + |S_2|^2 + |S_3|^2 + |S_4|^2\right), \tag{2.90}$$

and

$$S_{12} = \tfrac{1}{2}\left(|S_2|^2 - |S_1|^2 + |S_4|^2 - |S_3|^2\right), \tag{2.91}$$

as done by Bohren and Huffman [10].

The scattering amplitude matrix is a matrix that transforms the incoming electric field into the scattered electric field.

$$\begin{pmatrix} E_{\parallel s} \\ E_{\perp s} \end{pmatrix} = ie^{i\mathbf{k}_s\cdot\mathbf{r}-i\omega t} \begin{pmatrix} S_2 & S_3 \\ S_4 & S_1 \end{pmatrix} \begin{pmatrix} E_{\parallel i} \\ E_{\perp i} \end{pmatrix} \tag{2.92}$$

In order to do this, both the incoming electric field $\mathbf{E}_i$ and the scattered field $\mathbf{E}_s$ need to be divided into two components, one parallel to the scattering plane, $E_{\parallel s}$ and $E_{\parallel i}$, and and the other parallel to it, $E_{\perp s}$ and $E_{\perp i}$. All of these components are also perpendicular to their respective wave vectors $\mathbf{k}_s$ and $\mathbf{k}_0$.

The scattering amplitude matrix elements S_i can be calculated by following Draine and Flatau [8] and using

$$S_1 = \frac{2\pi}{k_0 L_y L_z \hat{x}\cdot\bar{k}_s}\hat{e}_{s\perp}\cdot\bar{F}_{TUC}(\hat{k}_s, \bar{E}_0 = \hat{e}_{i\perp}) \tag{2.93}$$

$$S_2 = \frac{2\pi}{k_0 L_y L_z \hat{x}\cdot\bar{k}_s}\hat{e}_{s\parallel}\cdot\bar{F}_{TUC}(\hat{k}_s, \bar{E}_0 = \hat{e}_{i\parallel}) \tag{2.94}$$

$$S_3 = \frac{2\pi}{k_0 L_y L_z \hat{x}\cdot\bar{k}_s}\hat{e}_{s\parallel}\cdot\bar{F}_{TUC}(\hat{k}_s, \bar{E}_0 = \hat{e}_{i\perp}) \tag{2.95}$$

$$S_4 = \frac{2\pi}{k_0 L_y L_z \hat{x}\cdot\bar{k}_s}\hat{e}_{s\perp}\cdot\bar{F}_{TUC}(\hat{k}_s, \bar{E}_0 = \hat{e}_{i\parallel}). \tag{2.96}$$

For example, S_2 is the portion of $E_{\parallel i}$ that contributes to $E_{\perp s}$ and so on. Looking at Eq. (2.92) it is easy to convince oneself that this indeed gives the right S_i. The unit vectors that are either parallel or perpendicular to the scattering plane and perpendicular to their

respective wave vectors $\mathbf{k}_0$ and $\mathbf{k}_s$ are defined as

$$\hat{e}_{i\perp} = \hat{e}_{s\perp} = \frac{\hat{k}_s \times \hat{k}_0}{|\hat{k}_s \times \hat{k}_0|} \tag{2.97}$$

$$\hat{e}_{i\parallel} = \hat{k}_0 \times \hat{e}_{i\perp} \tag{2.98}$$

$$\hat{e}_{s\parallel} = \hat{k}_s \times \hat{e}_{s\perp}. \tag{2.99}$$

Knowing this and the definitions of the Stokes vector and the amplitude scattering matrix (2.92) it becomes easy to derive the Mueller matrix elements (2.90) and (2.91).

Transmittances on the other hand can be calculated for the different orders of diffraction with the formula

$$T_{\alpha\beta}(M,N) = \frac{\sin\alpha_s}{\sin\alpha_0} S_{\alpha\beta}, \tag{2.100}$$

using the $S_{\alpha\beta}$ that correspond to scattering angles that go through the target. When the same is done with the angles and $S_{\alpha\beta}$ that correspond to reflections, one gets the reflectance $R_{\alpha\beta}(M,N)$. In cases where the incoming wave is perpendicular to the surface of the target, the transmittances and reflectances reduce to

$$T_{\alpha\beta}(M,N) = \frac{|k_{sx}|}{|k_{0x}|} S_{\alpha\beta} = S_{\alpha\beta}\cos\theta \tag{2.101}$$

$$R_{\alpha\beta}(M,N) = S_{\alpha\beta}\cos\theta, \tag{2.102}$$

because

$$\sin\alpha_s = \frac{|k_{sx}|}{k_0} \tag{2.103}$$

and

$$\sin\alpha_0 = \frac{|k_{0x}|}{k_0}. \tag{2.104}$$

The θ is simply the angle by which the scattering direction differs from the direction of the original wave vector $\mathbf{k}_0$. The matrices that are calculated with Eqs. (2.101) and (2.102) can be used like the Mueller matrix in Eq. (2.89) to get the portions of transmitted and reflected intensity from the incoming Stokes vector. Absorbance A is simply what is left of the incoming intensity once reflectance and transmittance are subtracted from it.

To sum up what is done in the discrete dipole approximation for periodic targets, first the volume integral equation which results from Maxwell's equations is discretized and solved using FFT and conjugate gradient method. This is done in order to find out

the polarizations $\bar{p}_i$ caused by the incoming wave in the target structure. A factor G is calculated to account for the periodicity of the target, and a matrix $\bar{F}_{TUC}$ is calculated from the polarizations. These can be either used to solve the electric field near the target or, with approximations, to calculate the elements of the scattering amplitude matrix S_i far away from the target, which in turn are used to calculate the elements of the Mueller matrix, which give the fraction of transmitted intensity for a given diffraction order.

Chapter 3

The Simulations

As mentioned before, the main idea of this thesis is to model the transfer of energy through a porous material via thermal radiation while taking into account the effects caused by the structure of the material. This is done by using a discrete dipole approximation program called DDSCAT, which was developed by Draine and Flatau [12][8][11]. Particularly, the version 7.1 of the code was used.

3.1 On the parameters

The parameters, which are necessary for DDSCAT 7.1 to work, are the complex dielectric function of the target, the target size and geometry, the angles, wavelengths and polarization of the incoming radiation, which Mueller matrices to calculate, orders of diffraction at which the Mueller matrix elements are calculated, the cut-off constant γ and the maximum allowed norm for the conjugate gradient method.

Interestingly, the physical lattice spacing of the dipoles, d is given with help of a parameter called the effective radius, a_{eff}. This effective radius is defined by Draine and Flatau [8] as $a_{eff} = (\frac{3N}{4\pi})^{1/3}d$, where N is the number of dipoles in one target unit cell.

Also it is necessary to specify that the target is periodic, however there will be more about the targets in the next section.

3.1.1 What was simulated

The targets were always approximately 6.4 μm thick layers of foam, where the walls between the bubbles were two dipoles, and so 80 nm thick, dipole spacing being 40 nm. This was done, so that especially the effect of the target geometry at wavelengths around and smaller than the target size could be observed.

Five different target geometries in total were used in the simulations. The simplest one was a 'cubical' foam where the bubbles in the foam were simple stacked 1.6 $\mu m \times 1.6$ $\mu m \times 1.6 \mu m$ cube shaped cavities in solid material. The target unit cells, of which the target plane consisted of, were four cube high stacks of cubical empty boxes made of dielectric material.

Three other target structures were variations of this where the cubes had been either stretched or flattened in the direction normal to the target plane, while attempting to keep the density, wall thickness and the thickness of the system constant. Specifically, two of these were 'stretched', with the size of the cavities having measures of 2.16 $\mu m \times 1.44$ $\mu m \times 1.44$ μm and target plane being three cavities thick on one, and on the other 3.2 $\mu m \times 1.28$ $\mu m \times 1.28$ μm cavities in a two cavity thick plane. The 'flattened' target had 1.28 $\mu m \times 1.84$ $\mu m \times 1.84$ μm cavities stacked five cavity high in the target plane. The target unit cells for these four structures can be seen in Fig. 3.1

The fifth target structure geometry was in the shape of the Kelvin structure, where the cavities are in the shape of truncated octahedra. It is named after its inventor Lord Kelvin, who conjectured the structure as a solution to how space can be partitioned so that all of the cells have equal volume, while minimizing the surface area between the cells [21]. The target unit cell for this structure can be seen in Fig. 3.2 The cavities had roughly the diameter of 1.6 μm. The size of the target unit cell was 6.4 $\mu m \times 1.6$ $\mu m \times 1.6$ μm, same as with the first 'cubical' target. Surprisingly the Kelvin structure also had the exact same density and as the first target. The wall thickness was only approximately same as in the other simulations for this last structure, because of the finite size of the dipoles that were simulated.

The Kelvin structure was used, because it is more realistic than a simple structure consisting of identical cuboids. What makes the Kelvin structure more realistic, is its close to minimal surfaces. Although a more ideal structure for minimal surfaces has been found by Weaire and Phelan [17], this structure, known as the Weaire-Phelan structure, is more complicated and probably for this reason the Kelvin structure seems to be more often used for modelling foams. The Kelvin structure has been in fact used before to model radiation in foams by, for example Tsang et al. [18], [19] and Miri et al. [20], but none of these used the discrete dipole approximation and either the size of the piece of structure that was modeled was always finite, or geometrical optics was used.

The complex dielectric function that was used for the target material in all of the simulations, was that of silicon-oxide in the form of glass [13]. Also the wavelengths that were simulated were same for all the targets, apart from some problematic lower wavelengths. The range of wavelengths that was covered reached from 0.8 μm to 10 μm. The planewave's wave vector was always perpendicular to the surface of the target plane. This is, because simulating all of the possible directions would have been prohibitively time consuming.

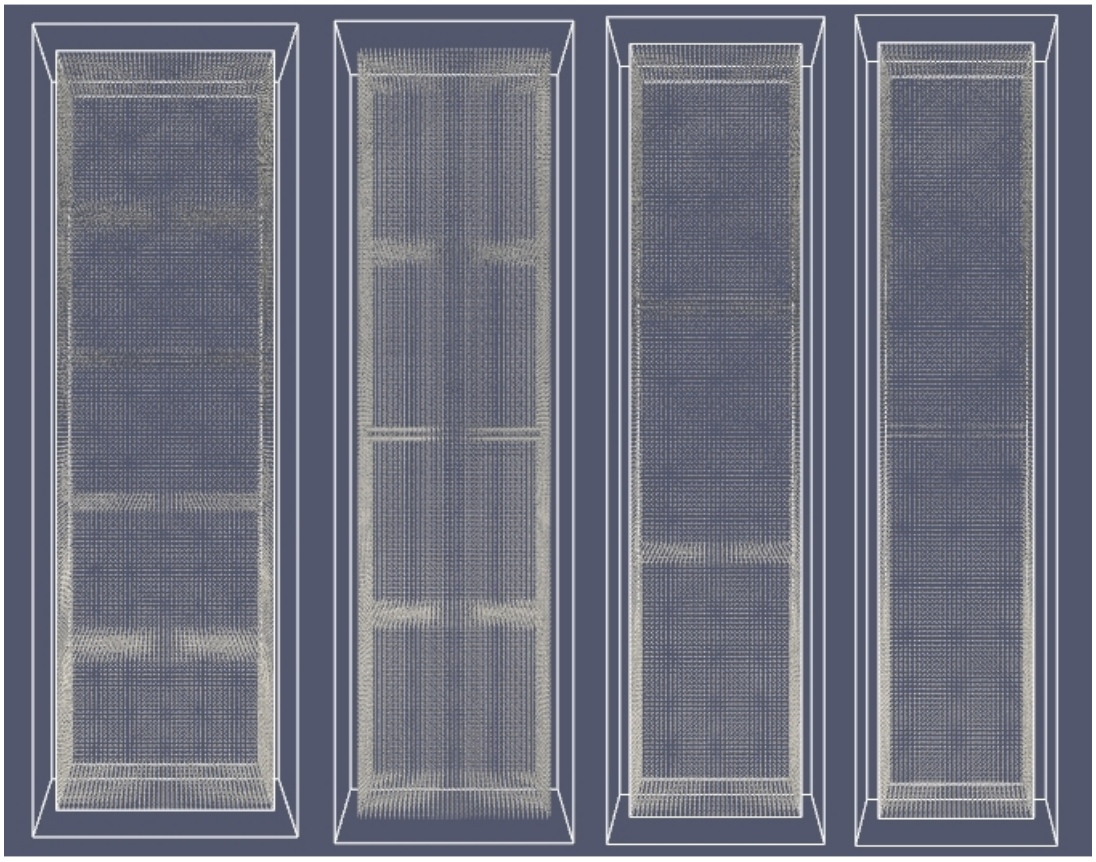

Figure 3.1: These are the target unit cells for the first four target structures. From left to right the sizes of the empty spaces in the structure are 1.28 $\mu m \times 1.84$ $\mu m \times 1.84$ μm, 1.6 $\mu m \times 1.6$ $\mu m \times 1.6 \mu m$, 2.16 $\mu m \times 1.44$ $\mu m \times 1.44$ μm and 3.2 $\mu m \times 1.28$ $\mu m \times 1.28$ μm. The walls between the empty spaces were 80 nm thick for all of the structures. The leftmost target unit cell consists of 48160 dipoles, while the others had a smaller number of dipoles.

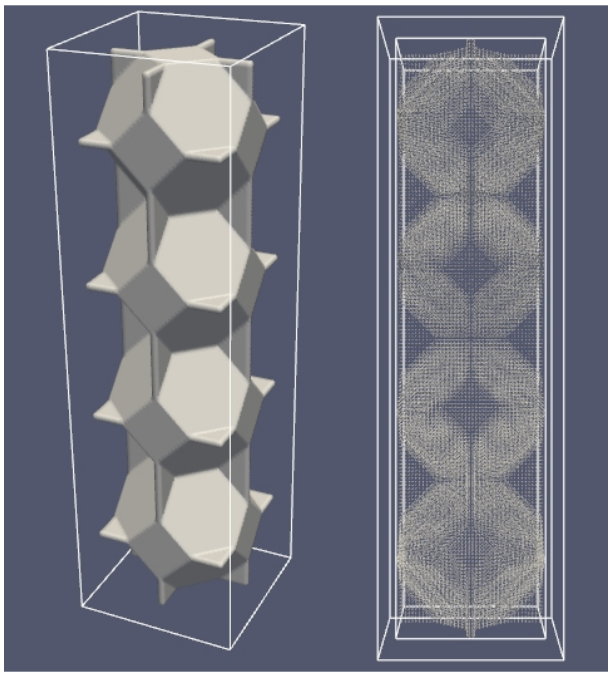

Figure 3.2: On the right is the target unit cell for the Kelvin structure, on the left is a picture where the surface of the target unit cell has been made solid to clarify on what the structure looks like. The surfaces on the actual Kelvin structure curve slightly, but due to finite number of dipoles this effect is not present in the target unit cell and all surfaces are flat.

It was found in the early simulations that the polarization of the wave didn't significantly affect the results, so to save time, only one polarization was used in the end. As for the cut-off parameter γ, the adviced value of 0.01 was used.

3.1.2 Limits of the parameters

When the wavelength of the incoming wave is large compared to the resolution of the system the time required for the simulation rises dramatically. Conversely, as the wavelength becomes closer to the dipole size in the system, error starts to appear in the results as the approximation starts to break down. Together these cause an upper and a lower limit for the wavelength, which limit the range of spectrum which can be covered by the simulations. Because Planck's distribution is very wide for low temperatures, this tends to limit the usefulness of the method to the larger temperatures.

Another limiting factor is the refractive index, or rather its relation to the dipole spacing d and the wavenumber k. According to Draine and Flatau [8], in their tests excellent accuracy compared to the analytical solution was achieved when the condition

$$|m|kd \leq 0.5 \tag{3.1}$$

was fulfilled. In other words, having too high of a refractive index can cause problems.

Also the number of dipoles that can be sensibly used in the simulation seems to be limited to the order of around 10^6 dipoles or less. If the desired target structure has, for example, very thin parts, which put a low upper limit to the size of the dipoles, the number of dipoles from which the structure is constructed may go too high.

Chapter 4

Results

DDSCAT was used to get the percentage of intensity that makes it through the sample for a given wavelength and angle of polarization. Only waves that were perpendicular to the sample were used. The differences in transmittance, reflectance and absorbance in the target structures can be seen in Figs. 4.1, 4.2 and 4.3. For such thin targets the transmittance seems to be much larger than the reflectance or absorbance. The reflectances are quite small in general, while the absorbances seem to largely follow the imaginary component of the complex index of refraction, this can be seen by comparing Fig. 4.3 with Fig. 4.4. Comparing the two pictures, one notices that for short wavelengths there seems to exist absorption even at wavelengths on which the material isn't capable of absorbing radiation, i.e. when the imaginary part of complex index of refraction is zero. Possible reasons for this are discussed later in Conclusions.

It is assumed that the incoming radiation takes the form of black body radiation and the incoming radiant energy is split into transmitted, reflected and absorbed parts. Because of the restrictions on which wavelengths can be simulated, some energy will always be unaccounted for. In the case where the temperature of the blackbody radiation source is $1000K$ and the range of wavelengths is from $0.9\mu m$ to $10\mu m$, the portion of energy which is covered by the simulation is 91.4%. This can be easily calculated using Stefan-Boltzmann law and Planck's law.

What happens to this covered part of the incoming radiant energy can be seen in Fig.4.5 and Table 4.1

These show that most of the energy is transmitted through the target. The amount of absorbed energy tends to be around 6% for all of the targets, while the portion of energy that is reflected varies between 1.5% to 0.16% from target to target.

Since for the smallest wavelengths, which were calculated with diffraction included, the targets absorbed radiation even when the material they were made of couldn't, it could be useful to look at a situation where this part of the spectrum is ignored. A

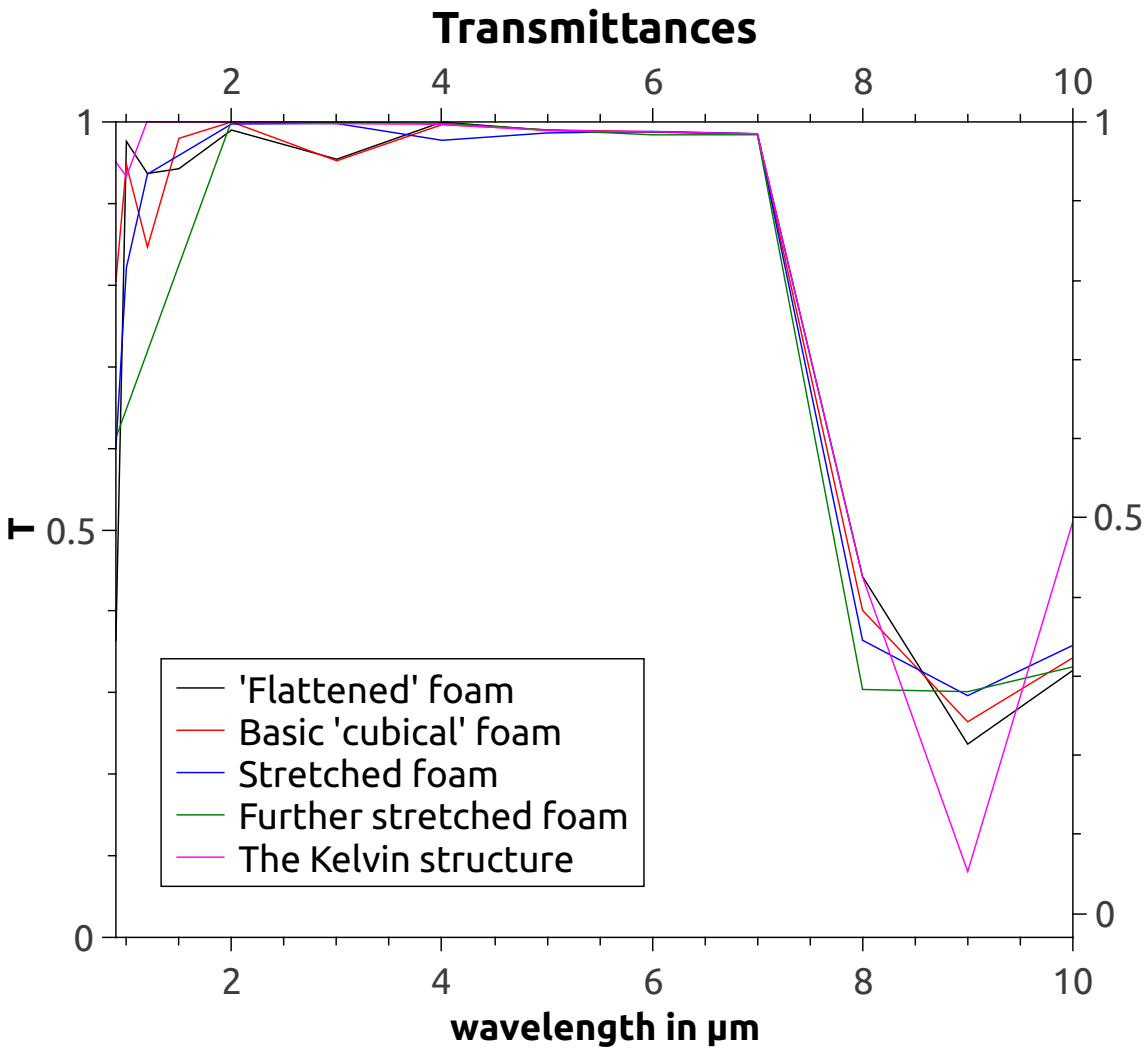

Figure 4.1: The transmittances for different wavelengths.

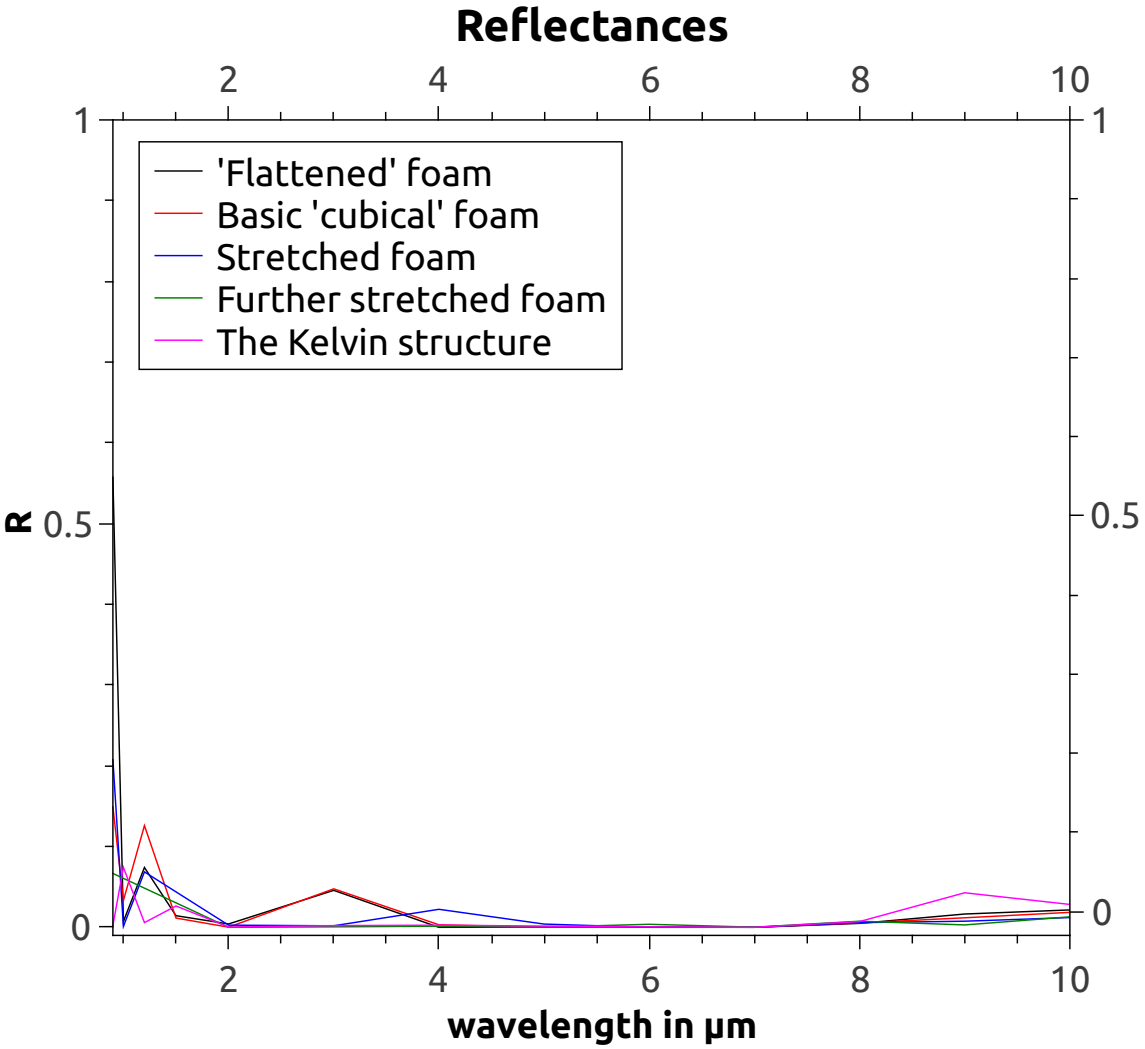

Figure 4.2: The reflectances for different wavelengths.

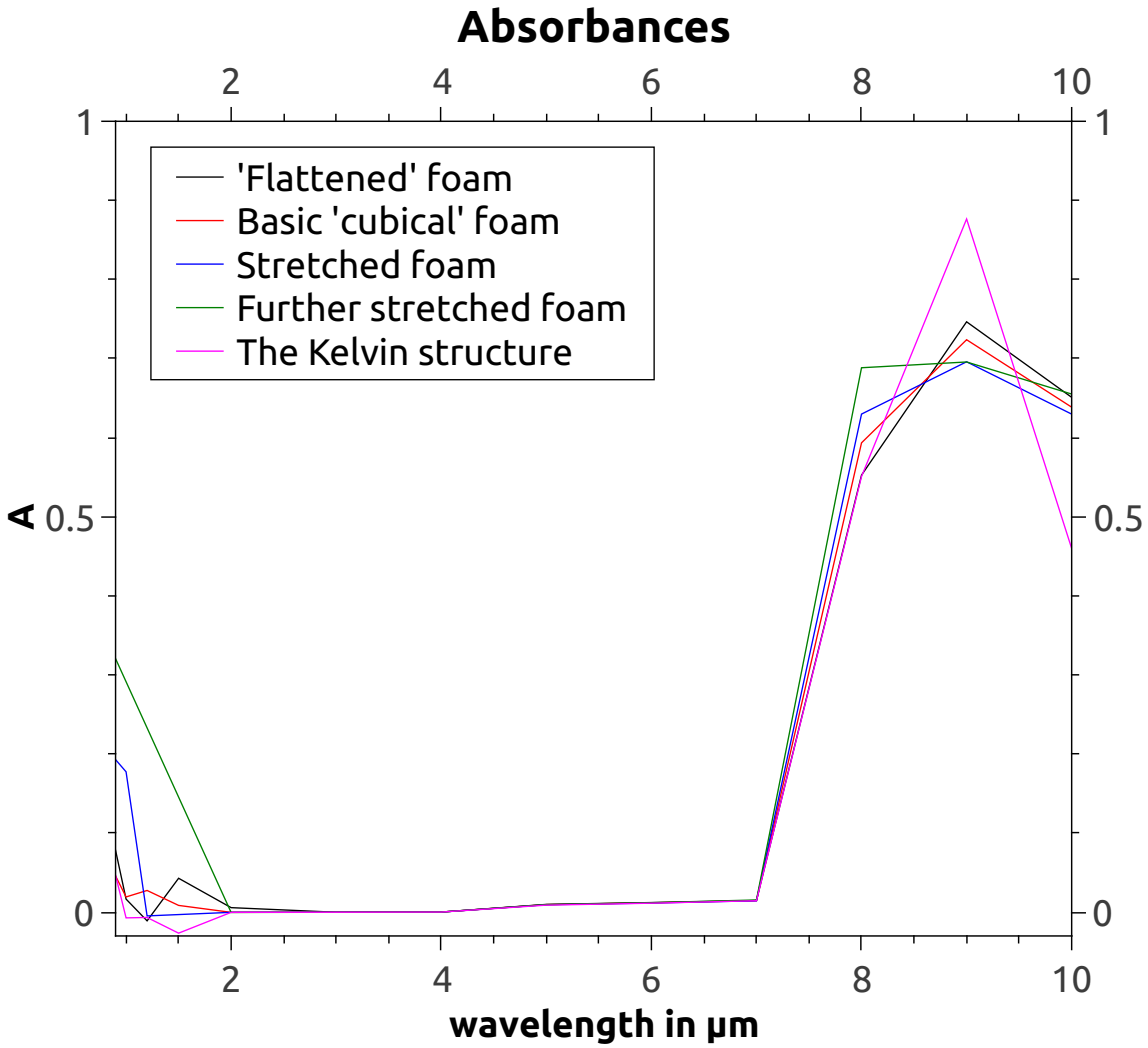

Figure 4.3: The absorbances for different wavelengths.

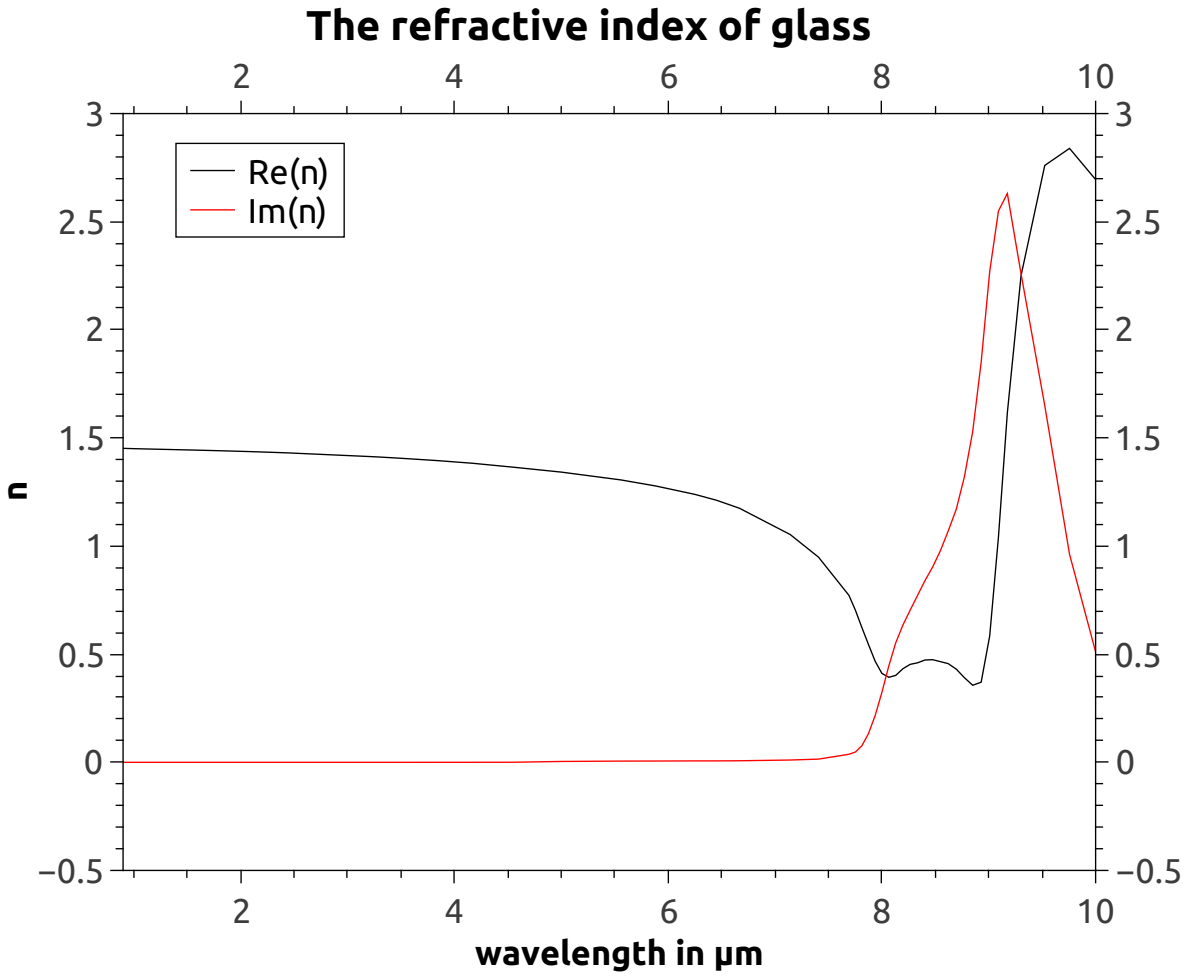

Figure 4.4: The complex refractive index of lime glass for different wavelengths.

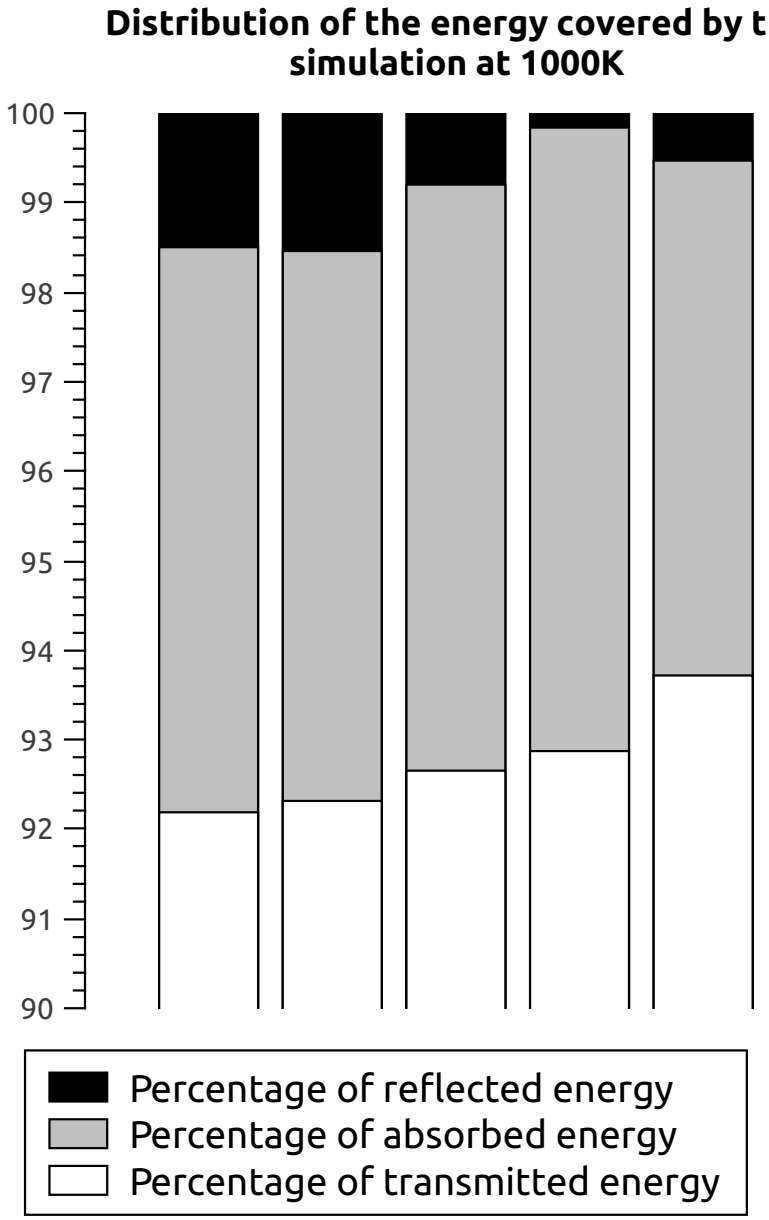

Figure 4.5: The target structures are from left to right: The "flattened" 1.28 $\mu m \times 1.84$ $\mu m \times 1.84$ μm cavity foam, the basic foam with 1.6 $\mu m \times 1.6$ $\mu m \times 1.6 \mu m$ cube shaped cavities, the stretched 2.16 $\mu m \times 1.44$ $\mu m \times 1.44$ μm cavity foam, the further stretched 3.2 $\mu m \times 1.28$ $\mu m \times 1.28$ μm cavity foam and finally the Kelvin structure. Note that the scale is from 90% to 100% instead of 0% to 100%, most of the energy is always transmitted.

The portions of incoming energy for 1000K

Target Structure	Transmitted	Reflected	Absorbed
"Flattened" foam	0.92189	0.014984	0.063131
Basic "cubical" foam	0.92316	0.015403	0.061437
Stretched foam foam	0.92654	0.0079743	0.065481
Further stretched foam	0.92873	0.0016113	0.069659
The Kelvin structure	0.93718	0.0052973	0.057522

Table 4.1: This table shows the portions of how much of the incoming energy, that is covered by the simulation, is transmitted, reflected and absorbed. The source is a blackbody with temperature of $1000K$.

The portions of incoming energy for 900K

Target Structure	Transmitted	Reflected	Absorbed
"Flattened" foam	0.9064	0.012327	0.081272
Basic "cubical" foam	0.90593	0.012629	0.081439
Stretched foam foam	0.91116	0.0068549	0.081987
Further stretched foam	0.91229	0.0017545	0.085955
The Kelvin structure	0.91597	0.0041998	0.079828

Table 4.2: This table shows the portions of how much of the incoming energy, that is covered by the simulation, is transmitted, reflected and absorbed. The source is a blackbody with temperature of $900K$.

new temperature for the blackbody radiator is needed, so that too much energy won't be outside of the scope of the simulation.

If the temperature of the radiation source is $900K$ and the spectrum ranges from $2\mu m$ to $10\mu m$, 85.1% of the energy is covered by the simulation. The result can be seen in Fig.4.6 and Table 4.2.

The biggest differences between Figs. 4.5 and 4.6 are mainly in the absorbed energy. This could be because the peak of blackbody radiation is closer to the absorptive area in the materials complex refractive index. Also, a bit less energy is reflected in the $900K$ cases. This could be because, as can be seen in Fig. 4.2, a lot of the reflecting happens in the beginning of the spectrum, which is cut off.

Another thing that can be seen from Figs. 4.5 and 4.6 is that the more elongated the cavities are the less energy is reflected. This could be expected, because many thin sheets of glass reflect light better than one thick sheet of glass would. However, looking

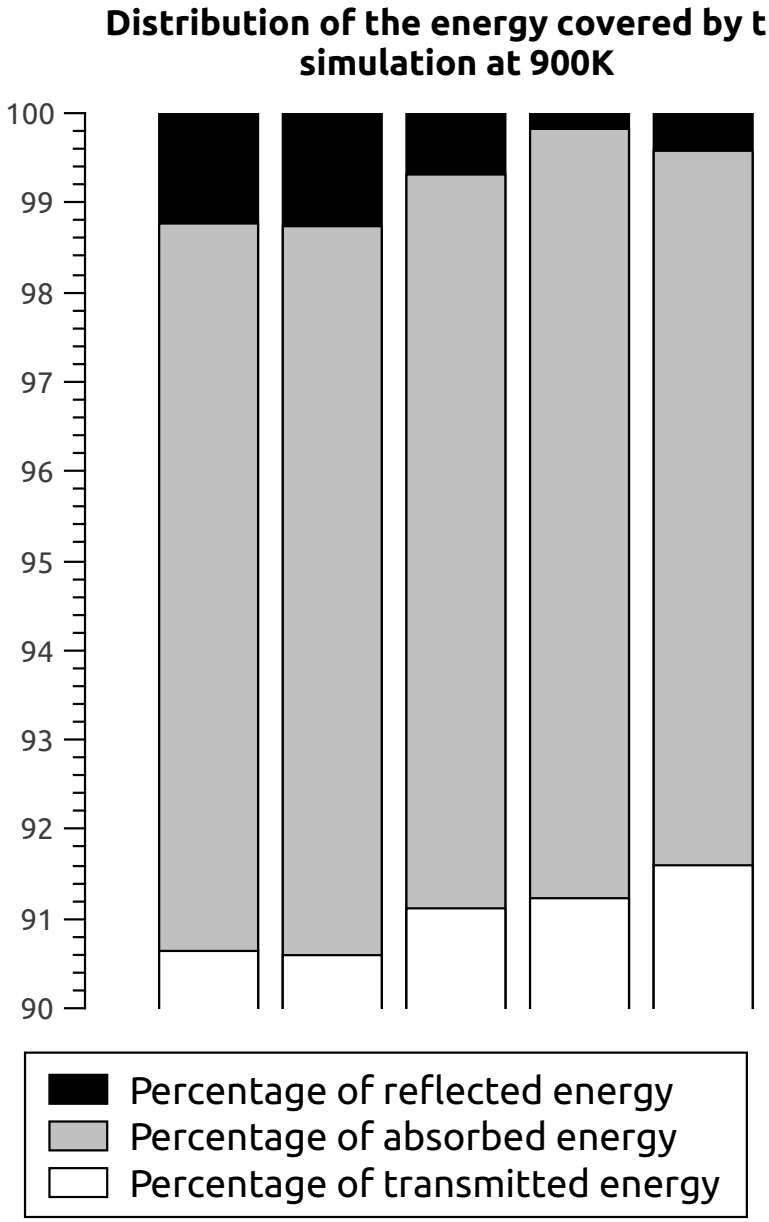

Figure 4.6: The target structures are from left to right: The "flattened" 1.28 $\mu m \times 1.84$ $\mu m \times 1.84$ μm cavity foam, the basic foam with 1.6 $\mu m \times 1.6$ $\mu m \times 1.6 \mu m$ cube shaped cavities, the stretched 2.16 $\mu m \times 1.44$ $\mu m \times 1.44$ μm cavity foam, the further stretched 3.2 $\mu m \times 1.28$ $\mu m \times 1.28$ μm cavity foam and finally the Kelvin structure. Again, the scale is from 90% to 100% instead of 0% to 100%. Most of the energy is always transmitted.

at the reflectances at different wavelengths presented in Fig. 4.2 might suggest a different reason.

As mentioned before, the heights of the cavities in the different target structures are $1.28\mu m$, $1.60\mu m$, $2.16\mu m$ and $3.20\mu m$. The structures with cavity heights of $1.28\mu m$ and $1.60\mu m$ seem to have a slight peak in reflection at around $3\mu m$, which is very roughly speaking about double the height of the cavities. Also the structure with cavity height of $2.16\mu m$ has a slight peak in reflection at around $4\mu m$, which is again in very rough approximation about double the height of the cavities. It could be that the part of the wave that reflects from the roof of the cavity and the part that reflects from the bottom of the cavity constructively interfere to increase reflectance in these cases. There is no corresponding reflectance peak for the $3.20\mu m$ structure, though this could be because it would lie between measurements at $6\mu m$ and $7\mu m$, or simply because the number of cavities is smaller. This would also explain why the peak for the $2.16\mu m$ cavity structure is shorter than the two previous ones.

To test this hypothesis, a new set of simulations was run using a target structure that simply consisted of a stack of 5 thin infinite sheets of the material. The sheets were set to be at intervals of $1.60\mu m$, so as to mimic the cubic structure, except without the vertical walls of the cubes. The comparison of the reflectances of the cubic structure, the sheet structure and the Kelvin structure can be seen in Fig. 4.7.

The sheet structure's reflectance seems to spike for wavelengths close to the gap between the sheets. This doesn't directly contradict the hypothesis that the bumps in the graphs could be caused by constructive interference, but it is puzzling that for the sheet structure the same wavelength which had the most reflection for the cubic structure, no produces almost no reflection at all.

The Kelvin structure on the other hand is most reflective at the end of the spectrum, and no peak in reflectance is seen to correspond to the structure with $1.60\mu m$ cube shaped cavities. Since the Kelvin structure is the most realistic of the target structures used, this implies that constructive interference probably isn't an effect that can be seen in real naturally formed foams in any case.

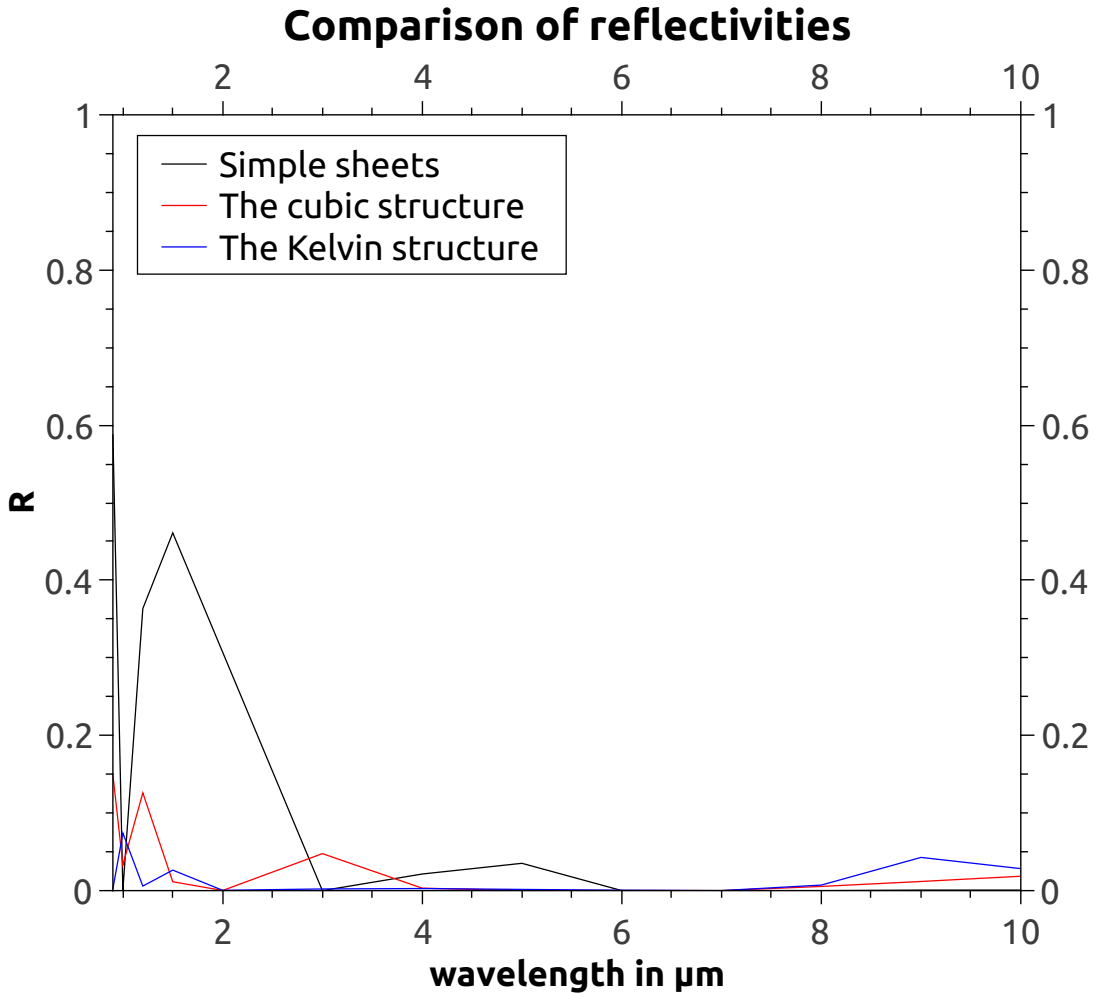

Figure 4.7: A comparison of the reflectances of the original cubic structure, the Kelvin structure and a structure consisting of 5 sheets of glass.

Chapter 5

Conclusions

5.1 Discussion on the error in small wavelengths

It is noteworthy that for the cases where diffractions are included, each diffraction needs its own simulation and so the error also grows together with the number of diffractions included. This helps understanding why there is so much error in the beginning of the spectrum where the diffractions happen.

The condition (3.1) was fulfilled for all of the simulations, so it isn't an obvious error source, though still a possible one. The condition may not be sufficient for all structures.

The cut-off parameter γ, which affects how far away one dipole's field is still considered significant for the calculation, is another thing that can affect accuracy. This was tested by running the simulation with γ set to 0.001 instead of the usual 0.01, but no significant change in error was found.

One possible error source can be found from a paper by Gutkowicz-Krusin and Draine [9], whose method of calculating the polarizabilities for the dipoles was used in the simulations. Apparently the only use for a high dipole count isn't to successfully replicate the shape of the target structure, but also the structures need to have sufficient thickness to negate surface effects regarding the polarization of the matter. More specifically, unlike on the surface, inside the target matter the outside field is screened by the surrounding polarized dipoles. If the target structure is only few dipoles thin, then a bigger portion of the matter faces the outside field unscreened and this can cause absorption to become exaggerated.

In the simulation the walls between cavities were for most cases only two dipoles thick, and so this may have been enough to cause some inaccuracy in the absorption, specifically at short wavelengths. However, the effect should mainly be an issue for large indices of refraction and it still doesn't explain why absorption happens when the imaginary part of the complex index of refraction is exactly zero.

In conclusion, no certain explanation was found for the error in absorption in short wavelengths. It is likely that the error is related to some part of the calculation process, that doesn't agree with certain target structures. It doesn't seem probable that this "inexplicable" absorption would have some physical explanation.

5.2 To sum up

Different methods for modeling thermal radiation in porous structures were discussed, with special interest on how the shape of the structure is taken into account in the model. In the end discrete dipole approximation was chosen for the simulation of scattering and absorption of radiation in periodic porous model structures. This method was chosen, because it allows the simulation of structures that are in size equal to or smaller than the wavelength of the radiation and because software that allows generalization for infinite repeating structures, namely DDSCAT, existed.

It was found that the biggest factor concerning absorption is the imaginary part of the complex index of refraction, while the shape of the structure does seem to affect reflection. It may be possible that for some of the simulated structures one of the processes affecting the reflections could have been constructive interference, however no conclusive evidence for this was found.

It was also found that significant error appeared for cases where the wavelength of the radiation was smaller than the period of the model structure. Possible reasons for this were discussed, but no definite answer was found.

Acknowledgements

I would like to thank senior researcher D. Sc. Ari Seppälä at the Applied Thermodynamics research group of Aalto university for guidance on this work.

Bibliography

[1] Siegel, R., Howell, J.R., 1981: Thermal Radiation Heat Transfer, Second Edition. Hemisphere Publishing Corporation, Washington. Pages 453-354, 501, 25, 504, 18, 4.

[2] Kaviany, M., Singh, B.P., 1993: Radiative Heat Transfer in Porous Media. Advances in Heat Transfer, Vol. 23, 133-186

[3] Doermann, D., Sacadura, J.F., 1996: Heat Transfer in Open Cell Foam Insulation. J. Heat Transfer, Trans. ASME 118, 88-93.

[4] Placido, E., Arduini-Schuster, M.C., Kuhn J., 2005: Thermal properties predictive model for insulating foams. Infrared Physics & Technology 46, 219-231.

[5] Coquard, R., Baillis, D., Quenard, D., 2009: Radiative Properties of Expanded Polystyrene Foams. J. Heat Transfer, Trans. ASME 131, 127-145.

[6] Tsang, L., Kong, J.A., Ding, K.H., Ao, C.O., 2001: Scattering of Electromagnetic Waves, Numerical Simulations. John Wiley & Sons, Inc., New York.

[7] Tsang, L., Kong, J.A., Ding, K.H., 2000: Scattering of Electromagnetic Waves, Theories and applications. John Wiley & Sons, Inc., New York.

[8] Draine, B.T., Flatau, P.J., 2008: Discrete-dipole approximation for periodic targets: theory and tests. J. Opt. Soc. Am. A, Vol. 25, 2693-2703

[9] Gutkowicz-Krusin, D., Draine, B.T., 2004: Propagation of electromagnetic waves on a rectangular lattice of polarizable points. http://arXiv.org/abs/astro-ph/0403082

[10] Bohren, C.F., Huffman, D.R., 1998: Absorption and Scattering of Light by Small Particles. Wiley-VCH, New York. Pages 46-49, 63-65.

[11] Draine, B.T. Flatau, P.J., 2010: User Guide for the Discrete Dipole Approximation Code DDSCAT 7.1. http://arxiv.org/abs/1002.1505

[12] Draine, B.T. Flatau, P.J., 1994: Discrete-dipole approximation for scattering calculations. J. Opt. Soc. Am. A, 11, 1491-1499.

[13] Palik, E.D., 1998: Handbook of Optical Constants of Solids. Elsevier.

[14] Ebbesen, T.W., Lezec, H.J., Ghaemi, H.F., Thio, T., Wolff, P.A., 1998: Extraordinary optical transmission through sub-wavelength hole arrays. Nature, Vol. 391, 667-669

[15] Braun, J., Gompf, B., Kobiela, G., Dressel, M., 2009: How Holes Can Obscure the View: Suppressed Transmission through an Ultrathin Metal Film by a Subwavelength Hole Array. Physical Review Letters. 103

[16] Petrasch, J., Wyss, P., Steinfeld, A., 2007: Tomography-based Monte Carlo determination of radiative properties of reticulate porous ceramics. Journal of Quantitative Spectroscopy and Radiative Transfer. Vol. 105, Issue 2, 180-197

[17] Weaire, D., Phelan, R., 1994: A counter-example to Kelvin's conjecture on minimal surfaces. Philosophial Magazine Letters. Vol. 69, No. 2 107-110

[18] Xu, P., Tsang, L., Chen, D., 2005: Application of the multilevel UV method to calculate microwave absorption and emission of ocean foam with Kelvin's tetrakaidecahedron structure. Microwave and Optical Technology Letters. Vol. 45, No. 5, 445-450

[19] Chen, D., Tsang, L., Jin, Y-Q., 2003: Microwave emission and scattering of layered foam based on Monte Carlo simulations of dense media. Geoscience and Remote Sensing Symposium, IGARSS'03. Proceedings. IEEE International. Vol. 1., 336-338

[20] Miri, M., Madadi, E., Stark, H., 2005: Diffusive transport of light in a Kelvin foam. Physical Review E 72, 031111

[21] Lord Kelvin, 1887: On the Division of Space with Minimum Partitional Area. Philosophical Magazine 24 (151): 503

[22] Purcell, E.M., Pennypacker, C.R., 1973: Scattering and Absorption of Light by Nonspherical Dielectric Grains. The Astronomical Journal, 186: 705-714

[23] Draine, B.T., Goodman, J., 1993: Beyond Clausius-Mossoti: Wave propagation on a polarizable point lattice and the discrete dipole approximation. The Astronomical Journal, 405: 685-697